1976

Influence of turbidity on the stratification development of a deep water reservoir.

David Allen Prouty

Department:

INFLUENCE OF TURBIDITY ON THE STRATIFICATION DEVELOPMENT OF A DEEP WATER RESERVOIR

BY

DAVID ALLEN PROUTY, 1952-

A THESIS

Presented to the Faculty of the Graduate School of the

UNIVERSITY OF MISSOURI-ROLLA

In Partial Fulfillment of the Requirements for the Degree

MASTER OF SCIENCE IN MECHANICAL ENGINEERING

1976

Approved by

(Advisor)

ABSTRACT

The influence of turbidity on the diurnal temperature distribution and thermocline development in a deep water impoundment which is exposed to heating and cooling loads by convection, evaporation, and radiation is examined analytically. The diurnal behavior of the solar load, directional and spectral, is used with an isotropic multiple scattering model to simulate the attenuation of solar flux by turbid water. The diurnal behavior of the ambient temperature, humidity and wind speed were mathematically modeled to simulate the local (Phelps Co.) spring time of the year. The combined conduction and radiation energy transfer through the water was treated as a one dimensional problem and the governing energy equation was numerically solved through an explicit finite difference method. The resulting temperature distribution is significantly affected by the turbidity level of the water and the behavior is similar to the natural temperature distribution in water reservoir. The surface temperature, however, appears to be affected more directly by the ambient conditions and not by the turbidity level of the water.

ACKNOWLEDGEMENTS

The author wishes to thank Dr. Armaly for his patience and guidance in the preparation of this work, and Dr. Look and Dr. Ho for their review of it.

The author is grateful to the Mechanical Engineering Department for support as a graduate teaching assistant, and as a graduate research assistant. Thanks is also due to the National Science Foundation for support under grant ENG75-06237, and the Water Resources Board for support under grant USDI-OWRT A 080-MO.

The author would finally like to thank his parents, and friends for their help during the preparation of this work.

TABLE OF CONTENTS

Table of Contents (continued)

LIST OF FIGURES

NOMENCLATURE

A_s	surface area
C	wind speed coefficient
C_a	water vapor concentration at the air side of the interface
C_p	specific heat
C_w	water vapor concentration at the water side of the interface
E_k	energy input by the wind
E_p	buoyant energy
$F_c(t)$	energy transfer due to convection
$F_d(t)$	energy transfer due to diffuse incident radiation
$F_{rad}(t)$	energy transfer due to radiation
$F_s(t)$	energy transfer due to surface emission
$F_v(t)$	energy transfer due to evaporation
$F_\lambda^+(x,\theta)$	monochromatic flux distribution in the positive direction
$F_\lambda^-(x,\theta)$	monochromatic flux distribution in the negative direction
$F_\lambda(\theta_o)$	monochromatic collimated incident radiation
g	gravitational constant
g_c	dimensionless constant
$H(x,t)$	divergence of the flux
h_c	convective heat transfer coefficient
h_m	mass transfer coefficient
K	thermal conductivity of water
K_a	thermal conductivity of air
L_e	Lewis number
n_λ	monochromatic index of refraction
P_a	partial pressure of water in air

P_o	partial pressure of water at water surface
R_w	gas constant
$S_\lambda(x)$	monochromatic source function
$T(x,t)$	temperature distribution
T_a	ambient temperature
T_i	initial temperature
t	time
t_m	time from midnight
t_s	time from sunrise
U	wind velocity
U^*	shear velocity on the air side of the interface
V^*	shear velocity on the water side of the interface
V_a	wind velocity
x	depth
z	depth
α	thermal diffusivity
β_λ	monochromatic extinction coefficient
ε_a	atmospheric emissivity
ε_w	emissivity of water surface
θ	polar angle in water
θ_o	collimated incident polar angle
κ_λ	monochromatic absorption coefficient
λ	wavelength
μ	direction in water
μ_a	absolute viscosity
ρ	density of water
ρ_a	density of air

$\rho_\lambda(\theta)$	monochromatic interface reflectance
σ	Stefan Boltzman constant
σ_λ	monochromatic scattering coefficient
τ	shear stress
τ_λ	monochromatic transmittance
ψ	relative humidity
$\psi_\lambda(\theta_o)$	monochromatic incident flux due to collimated radiation at θ_o
ω_λ	monochromatic scattering albedo

I. INTRODUCTION

The temperature distribution and seasonal stratification of water reservoirs is of interest to the ecologist, hydraulic engineers and to reservoirs management personnel because the life cycle in these waters is strongly affected by the magnitude of solar radiation and the temperature at depth. The seasonal stratification in water reservoirs is harmful to many underwater species because the level of oxygen at lower depths decreases rapidly below the thermocline. Cold water species living at these depths will not rise to higher levels due to the higher temperatures, therefore they must find other suitable water bodies or die. There has been recently some interest to exploit this stratification behavior in the ocean for the production of power. In these instances it is desirable to maximize the temperature differential between the surface and lower levels. Whatever the desired effect may be, if one correctly understands the stratification process involved, one can design and operate water reservoirs more successfully to fulfill the necessary requirements.

The stratification process of a water reservoir will be influenced significantly by the magnitude and the spectral distribution of the solar load and by the optical properties of the water. In addition, it will be affected by the transient behavior of the ambient temperature, humidity and wind speed. Previous investigations of these phenomenon dealt only with long term behavior leaving the diurnal changes to be either neglected or averaged. Also the radiative energy transferred through the water was treated by very

simple models which neglects the spectral and the directional dependency of the radiative transfer process.

The objective of this study is to develop a more accurate radiative transfer model which will include the effect of scattering and absorption. With the help of this model the energy conservation equation will be used to examine the influence of turbidity and ambient conditions on the diurnal temperature and flux distribution in a water reservoir.

II. REVIEW OF LITERATURE

Photosynthesis is of critical importance to the continuation of life, since it is the only known way to directly convert solar energy into living matter. There are a tremendous amount of publications available on photosynthesis [1-4] and on the role of the solar energy and photosynthesis in the life cycle. Both the temperature and the energy level influence the rate of photosynthetic productivity. The energy level is affected by the solar load and by the optical properties of the water. The temperature level is affected by the above energy level and by the ambient conditions that interact with the interface.

A. STUDIES RELATED TO PHOTOSYNTHESIS

Some researchers have considered the process of photosynthesis in water [5-15] and established that only that portion of the solar spectrum which is between the 0.4 and 0.75 microms [5,6] is photosynthetically active. The minimum energy level required to sustain photosynthesis is in the range of 50-100 foot candles (or 2.3-4.4 watts/meter^2). The rate of photosynthetic productivity increases as the energy level increases until it reaches a maximum. For some plants the maximum productivity will occur when the energy level is as low as 500 foot candles and for others the productivity will peak at energy levels above 2500 foot candles. In all cases, however, as the solar energy continues to increase the rate of photosynthetic productivity will begin to decrease. For example at 10,000 foot candles (460 watt/m^2) the rate of photosynthesis may be only 5% to 10% of the maximum rate. By using these limits which have been

proposed by Ryther [6], a euphotic zone may be defined where the conditions are not prohibitive for photosynthetic production. Strickland [5] has presented a method for analyzing the penetration of solar radiation into the ocean and discussed the importance of considering the directional properties of the incident radiation and scattering. Wezernak, Lyzenga, and Polycyn [16] examined the development of various forms of chlorophyll, which are widely used as an index of the photosynthetic productivity. They also discussed the changes in the reflectance characteristics due to particles suspended in water. Their research results indicate that an accurate radiation model, which includes the directional properties of the air-water interface and the selective attenuation of radiation by the water and the scattering of radiation caused by suspension of particulate matter, is necessary for the understanding of the photosynthetic process in the water.

B. STUDIES RELATED TO TEMPERATURE DISTRIBUTION

Harleman and co-workers [17-19] did some laboratory measurements and developed analytical models for predicting the temperature distribution in water reservoirs. In most cases the interest was primarily placed on predicting reservoirs discharge temperature rather than stratification development. They modeled the total radiation flux according to Beer's law and considered only buoyant mixing in the water. They did not consider the diurnal variation of ambient conditions or solar load. Ou [20] examined the temperature distribution in a deep water reservoir while maintaining one convective term in the energy equation and permitting the diffusivity to vary with depth. He used a specified surface water temperature variation

instead of imposing physical boundary conditions such as convection, evaporation and radiation. The radiative flux of his model varied in a manner similar to the one used by Harleman. An integral method was applied by Orlob et. al. [21] to perform an energy balance on a reservoir for predicting its outlet water temperature. The diffusivity and radiative flux models were the same as those used by Ou [20]. All of the above studies used Beer's law to describe the radiative flux distribution in the water. Shonting [22], in his treatment of the same problem, considered all of the radiation load to be absorbed at the surface which resulted in unreasonably high surface temperatures.

More realistic radiative transfer models have been applied to this problem by Foster [23], Snider [24], Hill and Viskanta [25], and by Lepper [26]. Foster [23] developed a convective circulation model in the upper surface layer of the ocean. He assumed a periodic variation with time for the flux and used the sum of three exponential terms (decay with depth) that fit some measured underwater flux data. His model allowed for windmixing by using an effective thermal conductivity and diffusivity. His results show a variation of a few tenths of a degree in the surface temperature. Viskanta also used the concept of approximating the flux distribution by more than one exponential term in studies with Snider [24] and Hill [25]. He based his approximations on an exact development of radiative transfer in water with forward scattering. He carried both experimental and analytical studies to determine stratifications development and outflow temperature from water reservoirs. The directional behavior of the solar load and wind mixing were not

considered in the development. Lepper [26] examined both the diurnal flux and the temperature distribution in a deep clear (non-scattering) reservoir. Surface evaporation, convections, radiation and buoyant mixing were part of the model. That is the only study in which the optical properties of the water and the spectral and angular distribution of the solar load were used to generate (through analysis) the radiative flux and its attenuation in the water. This study includes the effects of various levels of scattering, wind mixing, and uses the exact divergence of the flux in the numerical solution, rather than an approximation.

C. ENERGY EXCHANGE AT INTERFACE

Energy exchange at the air-water interface affects strongly the temperature distribution and the solution of the energy equation. Several processes are simultaneously in progress at the interface; convection, absorption of radiant energy, emission of radiant energy, mixing and evaporation. Many investigators attempted to lump all these activities into one and predict energy exchange by using one exchange coefficient [27,28]. This is not an accurate method since it decouples the surface temperature from the interchange process and does not allow one to investigate a single interchange mechanism.

Most of the available literature on evaporation from reservoirs uses Fick's law. The analogy between the heat and the mass transfer is usually applied to evaluate the mass transfer coefficient. In one study [29], both the heat and the mass transfer coefficient were predicted from shear stress correlation. Pierson and Jackman [30] compared the accuracy of several available evaporation formulas. These formulas are more applicable to laboratory or well controlled

conditions rather than the uncontrolled natural conditions. Lambuex [31] generated working formulas relating evaporations from lakes to experimental pan evaporation data. Schooley [32] used the concept of diffusion sublayer thickness to compare evaporation from air-sea interface to laboratory measured data. All the above models and many others on evaporation, were summarized by Paily, et. al. [33].

Wind initiates surface mixing due to the shear stress which acts on the interface, and this affects the temperature profile in the water. Some investigators [20,21,34-46], have accounted for this type of mixing by using an effective eddy diffusivity that varies with depth. In general, however, the eddy diffusivities variation that were used were obtained by forcing the predicted temperature profile to agree with measured temperature profiles. This approach might give good correlation, however, it is not based on a sound physical development and could not be extended to predict performance in a new reservoir. In order to account accurately for the vertical mixing due to wind induced shear stress on an hourly basis it is necessary to use wind velocity profile to determine the shear stress at the surface and then solve the governing momentum equation for the velocity distribution in the water. This approach is complicated and its usefulness is questioned due to the lack of accurate boundary conditions. Liggett [37] examined the two dimensional horizontal circulation using the above approach for a given reservoir geometry. Other work in this area has been presented by Janowitz [38,39]. Stefan [40] used the work of Wu [41] in determining shear stress relations at smooth and rough air-sea interface in order to determine the energy dissipated by the wind in the water. In the approach

kinetic energy produced was balanced with the potential energy to determine the depth of the mixed layer resulting from the wind mixing.

D. OPTICAL PROPERTIES OF WATER

One other factor, which is important to this study, is the optical properties of the water such as: refractive index, absorption and scattering coefficients. These properties will play a major role in the determination of the radiative flux distribution.

There is a great deal of discrepancies [42-45] in the determination of the attenuation coefficients for distilled or pure water in the visible range. Much of this can be blamed on the difficulty of defining and obtaining pure water. Some of the differences, however, could possibly be attributed to the differences in the scattering between the samples. Very little work has been published on the properties of turbid water where scattering and attenuation coefficient are clearly separated. In most cases an overall attenuation coefficient is given and the absorption coefficient of distilled water are subtracted to yield the monochromatic scattering coefficient. It is questionable whether such a procedure is accurate since absorption could be caused by impurities in the water. Hulburt [45] measured the absorption and the scattering properties of natural water and listed values in the visible region of the spectrum for distilled, coastal, and bay water. He claims that for bay water, his most turbid sample, one can assume that the scattering coefficient is independent of wavelength. Fairchild [46] summarizes the literature dealing with the measurements and the prediction of the optical properties of water and reports these properties at various

depths for few lakes in the eastern United States. His deduced values are based on isotropic scattering and no particulate attenuation.

In this study, solar energy will be considered as collimated and its angle of incidence (time dependent) will vary in accordance with its daily behavior. Its magnitude and spectral distribution will be deduced from the irradiance at the top of the atmosphere [47,48] by using appropriate spectral atmospheric transmission coefficients [49,50]. The directional reflectance of the air-water interface will be evaluated through the Fresnel relations [51] and will be used to evaluate the reflected and the transmitted solar energy across the interface. Thermal and optical properties of water will be those of distilled and turbid water. Due to the lack of published values for the turbidity levels of natural water, this parameter will be analytically generated by increasing the scattering properties. The solar flux distribution will be treated on monochromatic basis through the transport equation to allow for multiple scattering. Ambient conditions such as temperature, humidity and wind speed will be modeled to resemble natural condition. Wind mixing will be treated as suggested by the proposed model of Stefan [40]. The above will be incorporated in the conservation of energy equation and boundary conditions to determine the diurnal temperature distribution in clear and turbid water reservoir.

III. MATHEMATICAL FORMULATION

Consider a deep clear water impoundment of large extent such that the energy transfer is only in the vertical direction. The problem becomes essentially one-dimensional. Thermal and optical properties of the water (scattering and absorption coefficient and refractive index) are considered as independent of temperature over the range of temperatures encountered and dependent on wave length. The initial temperature distribution is uniform, simulating early spring conditions for this local area (Phelps Co.). Water inflow and outflow are negligible and surface winds are small to the extent that the water surface can be considered as smooth. The water body is exposed to the diurnal solar load and exhibit convection, evaporation and radiation heat transfer from its interface. Under the above assumptions the transient energy equation governing the temperature distribution is given by,

$$\rho C_p T(x,t)/\partial t = K\partial^2 T(x,t)/\partial x^2 - H(x,t) \qquad (1)$$

in which H(x,t) is the divergence of the transmitted total radiative flux and T(x,t) the temperature, both of which are functions of position x as measured from the air-water interface, and time, t. The terms ρ, C_p, and K indicate density, specific heat, and thermal conductivity of the water, respectively. The initial condition is assumed to be that of uniform temperature,

$$T(x,0) = T_i \qquad (2)$$

At the air-water interface, energy is transferred by convection, $F_c(t)$, evaporation, $F_v(t)$, and radiation, $F_{rad}(t)$, as given by,

$$-K\partial T/\partial x(0,t) = F_v(t) + F_c(t) + F_{rad}(t). \tag{3}$$

Deep in the impoundment the temperature remains uniform at the initial value and the flux is given by,

$$\frac{\partial T(\infty,t)}{\partial x} = 0. \tag{4}$$

The difficulties associated with modeling the diurnal temperature distribution in a natural impoundment, through the solution of the above governing equation, is to accurately supply the behavior of the solar flux distribution, $F(x,t)$, in the water and the energy transfer components at the interface, Equation (3). These parameters depend on latitude, season, time of day, meteorological conditions and the impurities of the water. It will be difficult if not impossible to specify accurately these terms over a large area and for a long period of time. For that reason the models that are used in this study to predict these quantities are kept simple in order to simulate the trends of the diurnal behavior as discussed in sections VI and VII.

IV. ATTENUATION OF SOLAR FLUX BY TURBID WATER

For the case of semi-infinite isotropically scattering medium with refractive index, n_λ, larger than unity and with an incident radiation collimated at angle θ_o, $F_\lambda(\theta_o)$, on its interface Armaly and Lam [52] developed an algebraic expression for the monochromatic source function $S_\lambda(x)$ distribution given by:

$$S_\lambda(x) = \left[\frac{\omega_\lambda \psi_\lambda(\theta_o)[1 - \rho_{1\lambda}(\theta_o)]}{4\pi C_{o\lambda}}\right]\left[C_{1\lambda}\exp(-q\beta_\lambda x) + C_{2\lambda}\exp(-d_{o\lambda}\beta_\lambda x) + \frac{(1 - a^2C_{o\lambda}^2)\exp(-\beta_\lambda x/C_{o\lambda})}{(1 - d_{o\lambda}^2 C_{o\lambda}^2)}\right] \tag{5}$$

$$C_{o\lambda}^2 = 1 - (\sin\theta_o/n_\lambda)^2 \tag{6}$$

$$C_{1\lambda} = -\left[\frac{\omega_\lambda a^2 C_{o\lambda}}{(1 - C_{o\lambda}^2 d_{o\lambda}^2)d_{o\lambda}} + \frac{C_{o\lambda}(1 - a^2C_{o\lambda}^2)(d_{o\lambda} + q)}{(1 + C_{o\lambda}q)(1 + C_{o\lambda}^2 d_{o\lambda}^2)}\right] \Bigg/ \left[\frac{\omega_\lambda a^2 q}{d_{o\lambda}(q^2 - a^2)} + \frac{2(d_{o\lambda} + q)}{p\omega_\lambda}\left[1 + \frac{\omega_\lambda a^2}{(q^2 - a^2)} + \frac{\omega_\lambda p}{4q}\right]\right] \tag{7}$$

$$C_{2\lambda} = \left[\frac{\omega_\lambda a^2}{d_{o\lambda}}\right]\left[\frac{qC_{1\lambda}}{(q^2 - a^2)} + \frac{C_{o\lambda}}{(1 - C_{o\lambda}^2 d_{o\lambda}^2)}\right] \tag{8}$$

The above relations for $C_{1\lambda}$ and $C_{2\lambda}$ are not suitable for the conservative case or when ω_λ equal 1. For that case the following relations should be used.

$$C_{1\lambda} = C_{o\lambda}(a^2 - q^2)/q \tag{9}$$

and

$$C_{2\lambda} = -\left[\frac{2q}{p}\right]\left[C_{1\lambda}\left(1 + \frac{a^2}{(q^2 - a^2)} + \frac{p}{4q}\right) + \frac{C_{o\lambda}p(1 - a^2C_{o\lambda})}{2(1 + C_{o\lambda}q)}\right] \tag{10}$$

Where β_λ is the monochromatic extinction coefficient defined to be the sum of the scattering coefficient (σ_λ) and the absorption coefficient (κ_λ), ω_λ, scattering albedo, is the ratio of the scattering coefficient to the extinction coefficient, $\rho_{1\lambda}(\theta_o)$ is the monochromatic interface reflection due to radiation incident from the air side of the interface in the direction of θ_o and is calculated by using the Fresnel relations [51]. The constant "a" is the one used in the exponential approximation to the exponential integral [53] and has a value of a = 2 in this study. The other constants q and p are the ones used in the exponential kernel approximation to the interface function [54] and for water, the refractive index is 1.33. These constants have values of q = 1.177 and p = 0.375. The monochromatic flux at the interface due to collimated radiation in the direction of θ_o is given by:

$$\psi_\lambda(\theta_o) = F_\lambda(\theta_o) \cos \theta_o \tag{11}$$

Another constant is given by:

$$d_{o\lambda}^2 = a^2(1 - \omega_\lambda) \tag{12}$$

The intensity distribution through the medium was calculated using Equation (5) for the source function and the flux distribution was then evaluated from the intensity distribution as outlined in reference [52]. The expression for the flux distribution in the positive and negative directions, $F_\lambda^+(x,\theta_o)$ and $F_\lambda^-(x,\theta_o)$, were determined to be

$$\begin{aligned} F_\lambda^+(x,\theta_o) = \psi_\lambda(\theta_o)[1 - \rho_{1\lambda}(\theta_o)] \Bigg[& \exp(-\beta_\lambda x/C_{o\lambda}) \\ & + \frac{\omega_\lambda}{2C_{o\lambda}} \int_o^1 \Bigg\{ A_\lambda(\mu)\rho_\lambda(\mu)\exp(-\beta_\lambda x/\mu) \\ & + \frac{C_{1\lambda}}{\mu q - 1} \Big[\exp(-\beta_\lambda x/\mu) - \exp(-q\beta_\lambda x) \Big] \\ & + \frac{C_{2\lambda}}{\mu d_{o\lambda} - 1} \Big[\exp(-\beta_\lambda x/\mu) - \exp(-d_{o\lambda}\beta_\lambda x) \Big] \\ & + \frac{C_{o\lambda}(1 - a^2C_{o\lambda}^2)}{(1 - C_{o\lambda}^2 d_{o\lambda}^2)(\mu - C_{o\lambda})} \Big[\exp(-\beta_\lambda x/\mu) \\ & - \exp(-\beta_\lambda x/C_{o\lambda}) \Big] \Bigg\} \mu d\mu \Bigg] \end{aligned} \tag{13}$$

and

$$F_\lambda^-(x,\theta_o) = \left[\frac{\omega_\lambda \psi_\lambda(\theta_o)[1 - \rho_{1\lambda}(\theta_o)]}{2C_{o\lambda}}\right] \int_o^1 \left[\frac{C_{1\lambda}\exp(-q\beta_\lambda x)}{(\mu q + 1)}\right.$$

$$+ \frac{C_{2\lambda}\exp(-d_{o\lambda}\beta_\lambda x)}{(\mu d_{o\lambda} + 1)}$$

$$\left. + \frac{C_{o\lambda}(1 - a^2C_{o\lambda}^2)\exp(-\beta_\lambda x/C_{o\lambda})}{(1 - C_{o\lambda}^2 d_{o\lambda}^2)(\mu + C_{o\lambda})}\right] \mu d\mu \qquad (14)$$

$$A_\lambda(\mu) = \frac{C_{1\lambda}}{q\mu + 1} + \frac{C_{2\lambda}}{\mu d_{o\lambda} + 1} + \frac{(1 - a^2C_{o\lambda}^2)C_{o\lambda}}{(1 - C_{o\lambda}^2 d_{o\lambda}^2)(\mu + C_{o\lambda})} \qquad (15)$$

The parameter μ, a dummy variable in the integration, is equivalent to $\mu = \cos\theta$, where θ is the angular direction in the water. Notice that the interface reflectance for incident radiation from the water side of the interface in the direction of θ is given by $\rho_\lambda(\theta)$ and is calculated by using the Fresnel relations. The net monochromatic flux is given by

$$F_\lambda(x,\theta_o) = F_\lambda^+(x,\theta_o) - F_\lambda^-(x,\theta_o) \qquad (16)$$

and a monochromatic transmittance can be defined as the ratio of the local flux to incident flux, given by:

$$\tau_\lambda(x,\theta_o) = \frac{F_\lambda(x,\theta_o)}{\psi_\lambda(\theta_o)} \tag{17}$$

The influence of turbidity (i.e. changes in ω_λ) on the monochromatic transmission is presented as Figure 1 in the case of normal incident solar radiation. Analysis of this figure indicates that the increase of scattering albedo ω_λ while maintaining the extinctions coefficient constant will cause the net flux to decrease for small depth and it reverses that trend as the depth increases. At higher scattering levels the difference in magnitudes of the fluxes in the positive and negative directions becomes small causing the net flux and the transmittance to decrease rapidly.

The total flux is given by

$$F(x,\theta_o) = \int_o^\infty F_\lambda(x,\theta_o)\, d\lambda \tag{18}$$

and the divergence of the total flux which is the term appearing in the energy equation, Equation (36), is given by

$$H(x,\theta_o) = \frac{d}{dx} F(x,\theta_o) \tag{19}$$

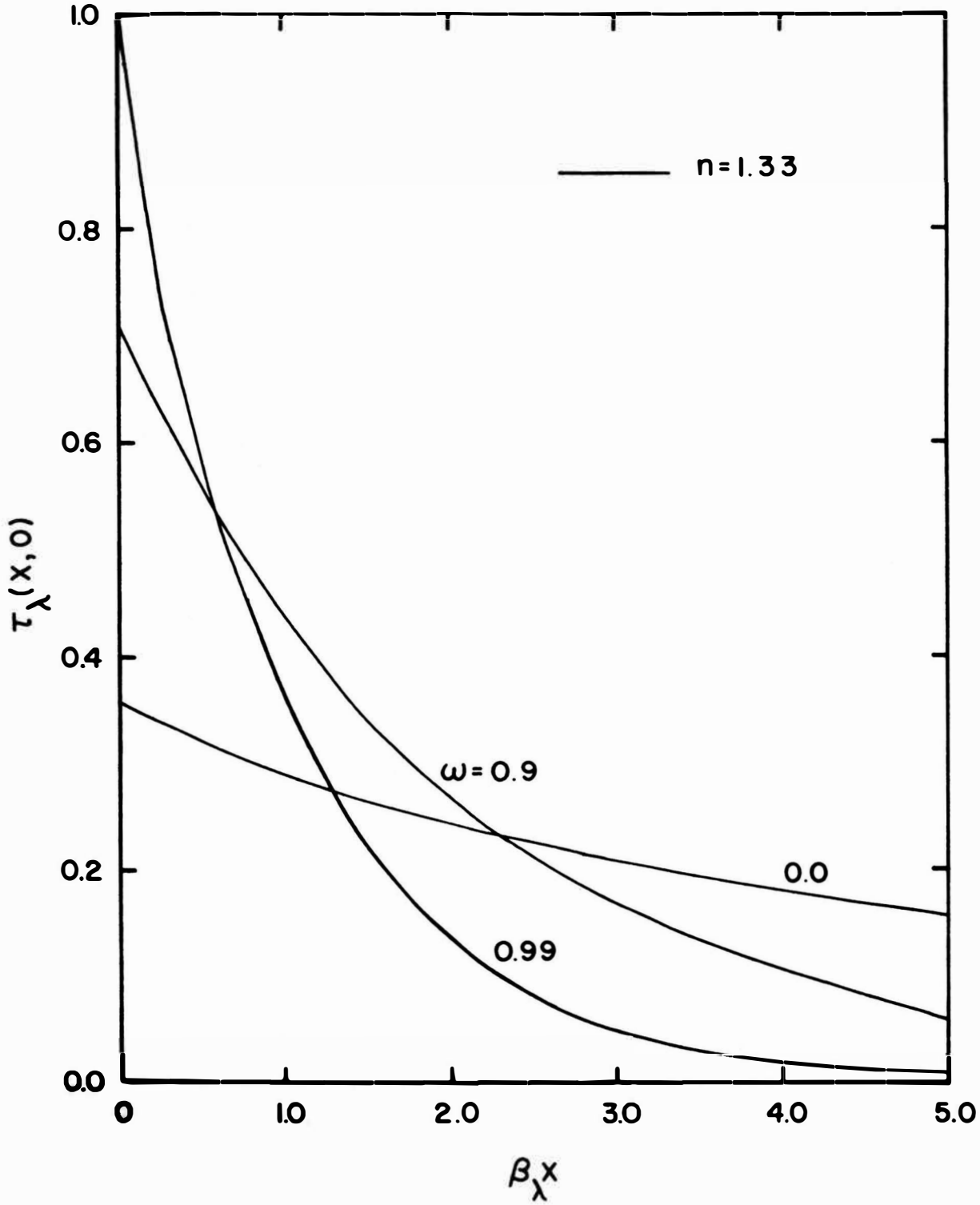

Figure 1. Monochromatic Transmittance of Normal Incident Collimated Radiation

V. OPTICAL PROPERTIES OF TURBID WATER

The attenuation of the solar flux through the water depends strongly on the magnitude of the spectral absorption and scattering coefficients. Unfortunately very little if any has been published on the magnitude of these properties for turbid water. In fact, there are descrepancies in the published values for distilled water [55]. Recently, Fairchild [46] reported on the measurements of the extinction coefficient for several natural water bodies. By using the assumption of isotropic scattering and no particulate absorption he deduced and reported the scattering coefficient of these water bodies. Optical properties of distilled water have been reviewed and analyzed in reference [56].

To examine the influence of water turbidity on the attenuation of the total solar flux, five different sets of optical properties were used to simulate different bodies of water and will be referred to as Cases 1 through 5. Case 1 uses the properties of clear non-scattering distilled water [55] shown in Figure 2. This case will be used as a reference to compare and judge the influence of increasing either the scattering or the absorption on the attenuation of the solar flux. Cases 2 and 3 represent the Yates and Benson ponds respectively for which Fairchild [46] reported the spectral absorption and scattering coefficients. Case 4 is an analytically generated model which is used to examine the influence of increasing the scattering coefficient, or simulating turbid water. Measurements by Hulburt [57] suggest that the scattering coefficient of turbid water is independent of wave length. The properties for Case 4 were then

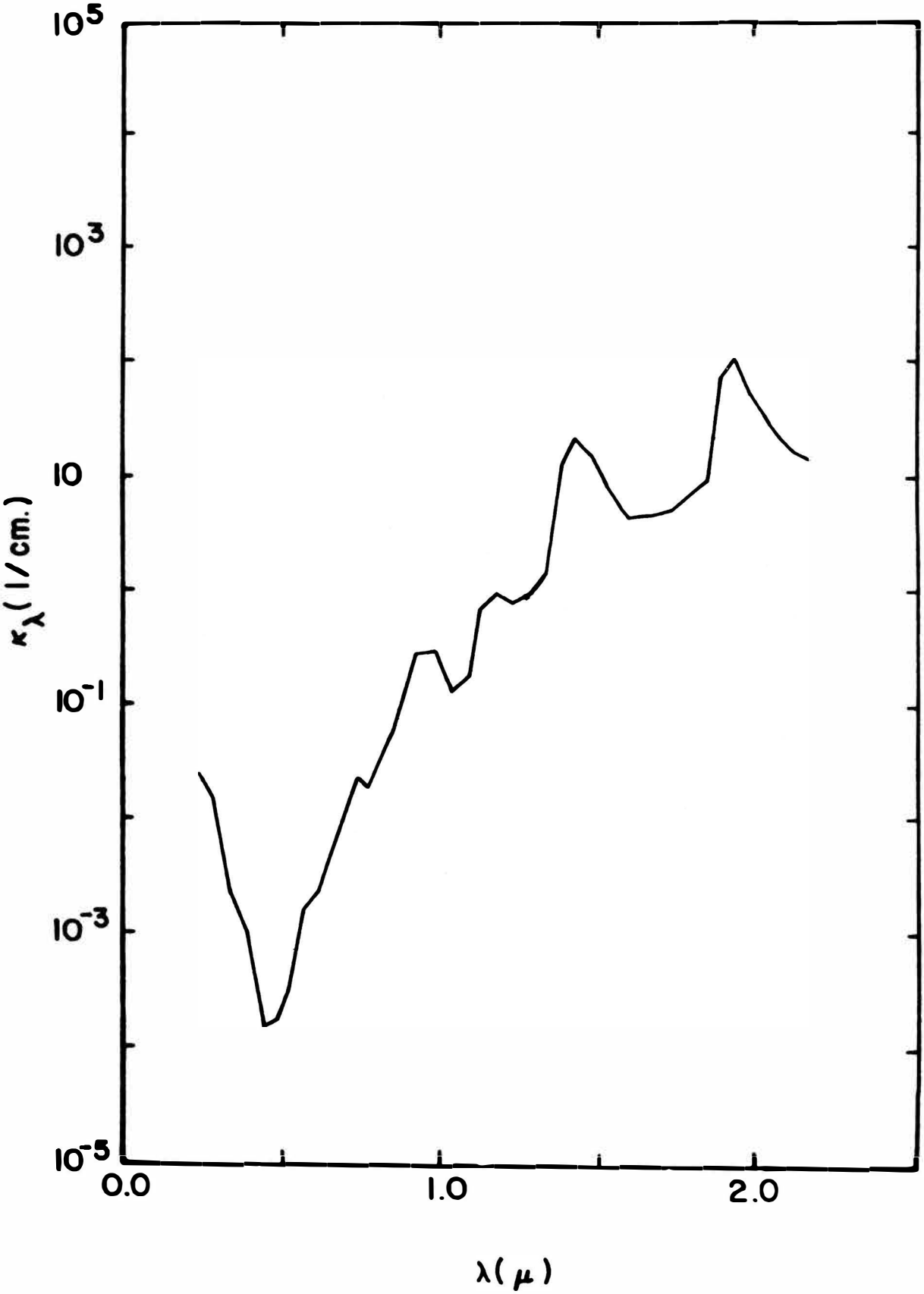

Figure 2. Absorption Coefficient for Distilled Water

generated from those of distilled water by increasing the scattering coefficient in a manner so as to maintain the extinction coefficient at constant value of 0.1 (1/cm) through the spectral range where its magnitude was smaller. Outside the spectral range its magnitude was maintained at the same values as that of distilled water. This procedure increased the extinction coefficient by more than two orders of magnitudes in the spectral region between 0.45 and 0.5 microns. Some inland turbid ponds indicate the above level of attenuation. Case 5 is also an analytically generated model which is used to examine the influence of increasing absorption, simulating dirty but non-scattering reservoir. The properties for Case 5 were generated by increasing the absorption coefficient of the Yates pond water [46] by one order of magnitude. The extinction coefficients for the five cases are shown as Figure 3. The scattering coefficient and the albedo for the cases 2, 3, 4 and 5, where scattering was part of the extinction coefficient, are presented in Figures 4 and 5 respectively.

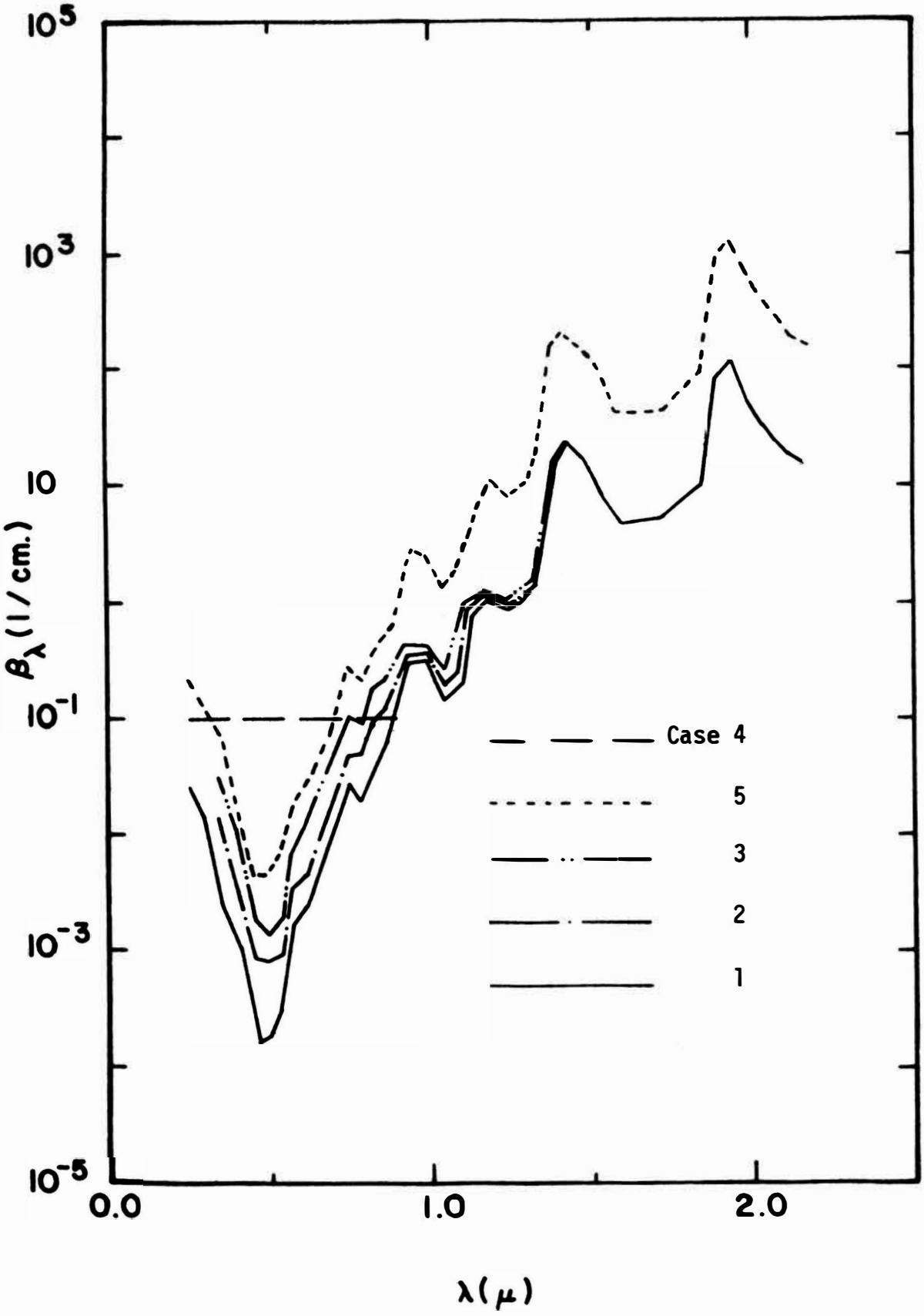

Figure 3. Extinction Coefficient of Turbid Water

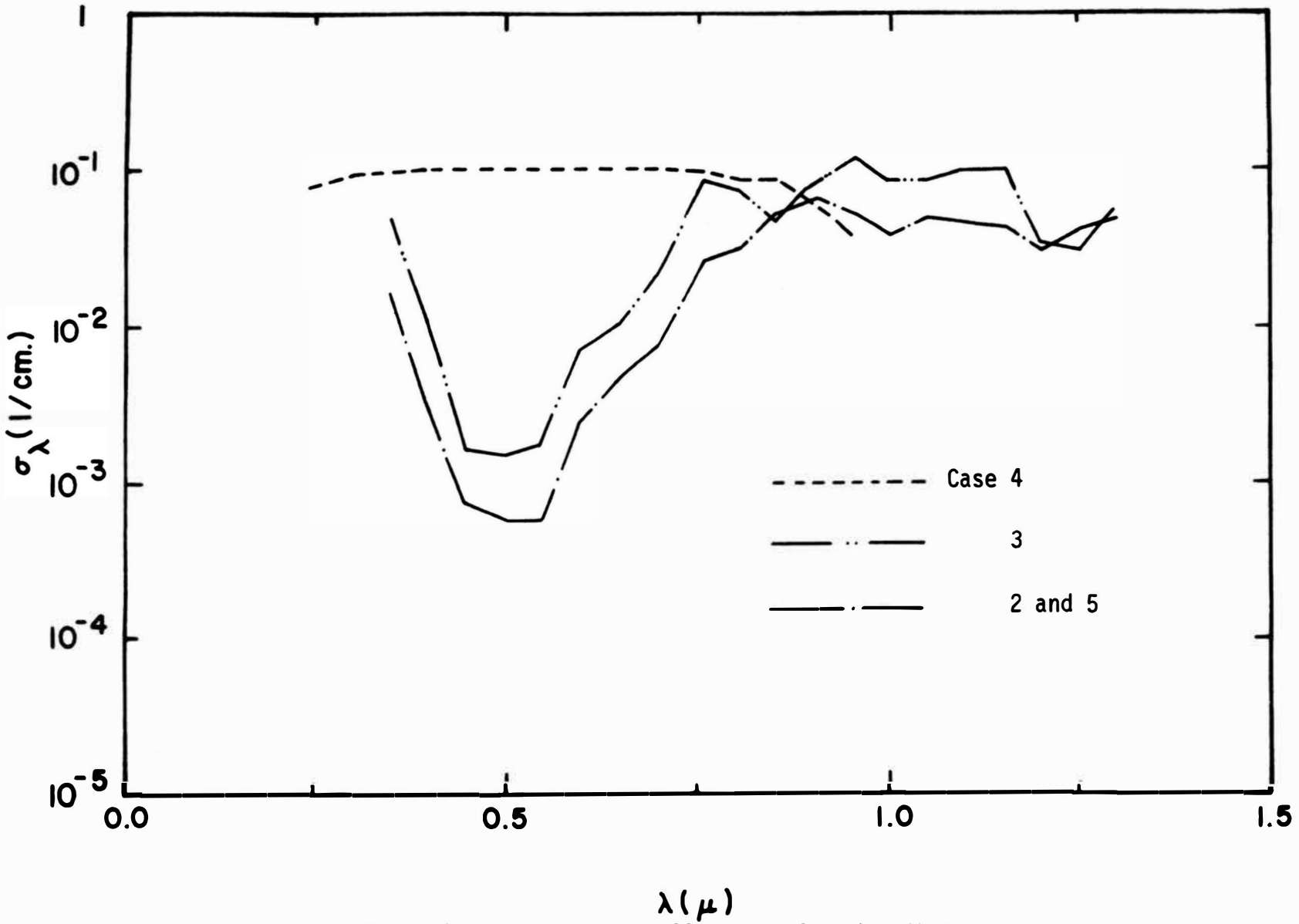

Figure 4. Scattering Coefficient of Turbid Water

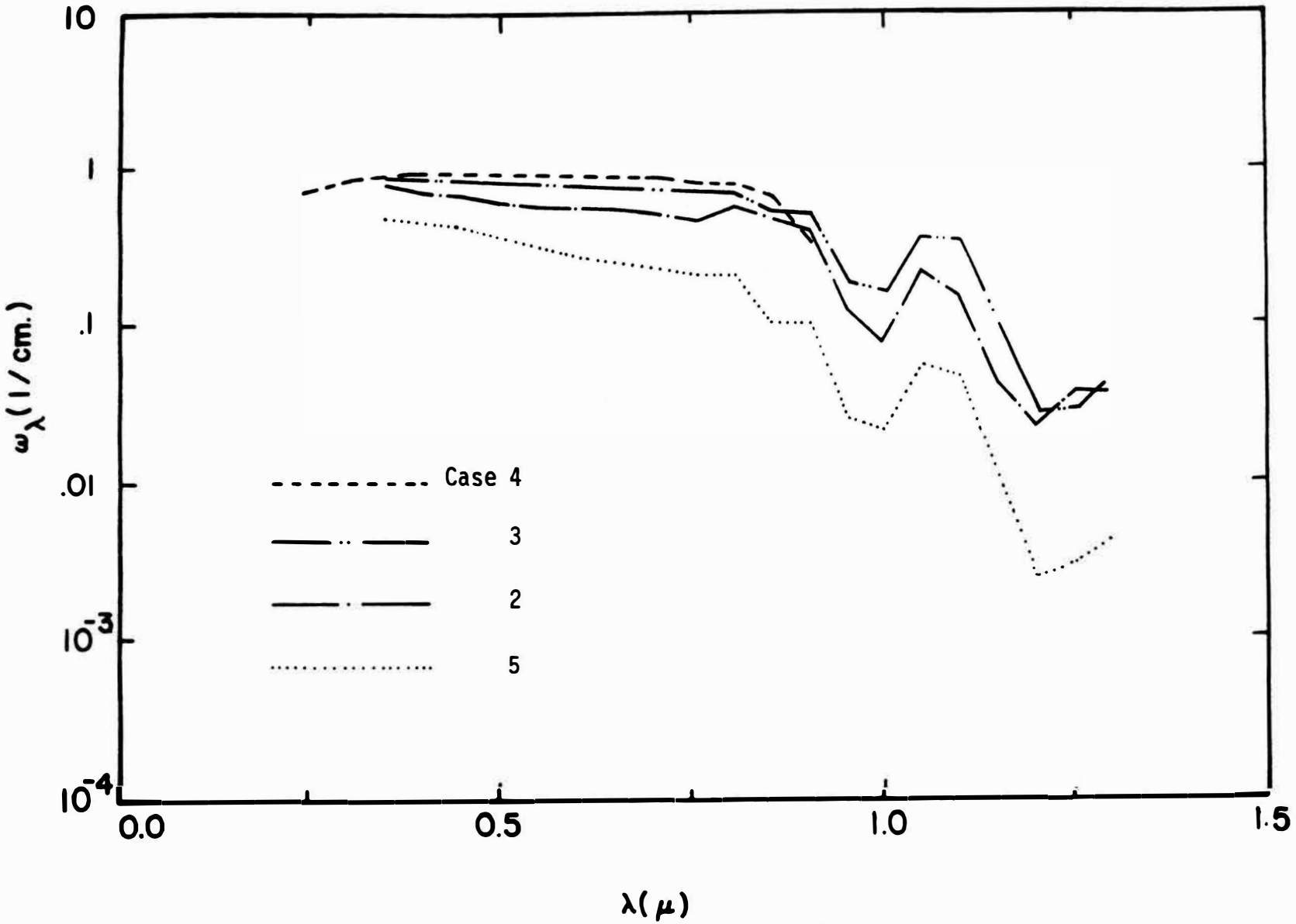

Figure 5. Scattering Albedo of Turbid Water

VI. DIURNAL SOLAR FLUX DISTRIBUTION

The monochromatic optical properties of the five water cases were used with directional and spectral solar load in an isotropic radiative transport model to evaluate the total diurnal solar flux and divergence distribution. The total flux distribution for each case is shown as Figures 6 and 7. The magnitude of the flux decreases with increasing incident angle because the solar load decreased, by the longer atmospheric path, and the rapid decrease of interface transmittance at larger angles. It can be observed from these figures that changes in the optical porperties of water significantly affect the attenuation of solar radiation.

As expected, an increase in the absorption coefficient, Case 5, causes a significant drop in the transmitted total flux (about 12 percent in the first tenth of a centimeter at normal incident). It did not change significantly the rate of change with depth (divergence) until the depth is below one meter. An increase of the scattering coefficient, on the other hand, Case 4, raises the divergence significantly in the upper layers (to depth of one-half meter) and therefore causes the rapid decline in the magnitude of the total flux. The divergence of the flux for all cases is presented in Figures 8 and 9. The curves for the first three cases are approximately the same up to depths of one meter, then the effect of scattering begins to show up (the more turbid cases drop faster). The highly turbid water, Case 4, had the fastest decrease with depth and Case 5 had the largest divergence at the surface. The angle of incident does not seem to change the relative shape of the curves, only the magnitude.

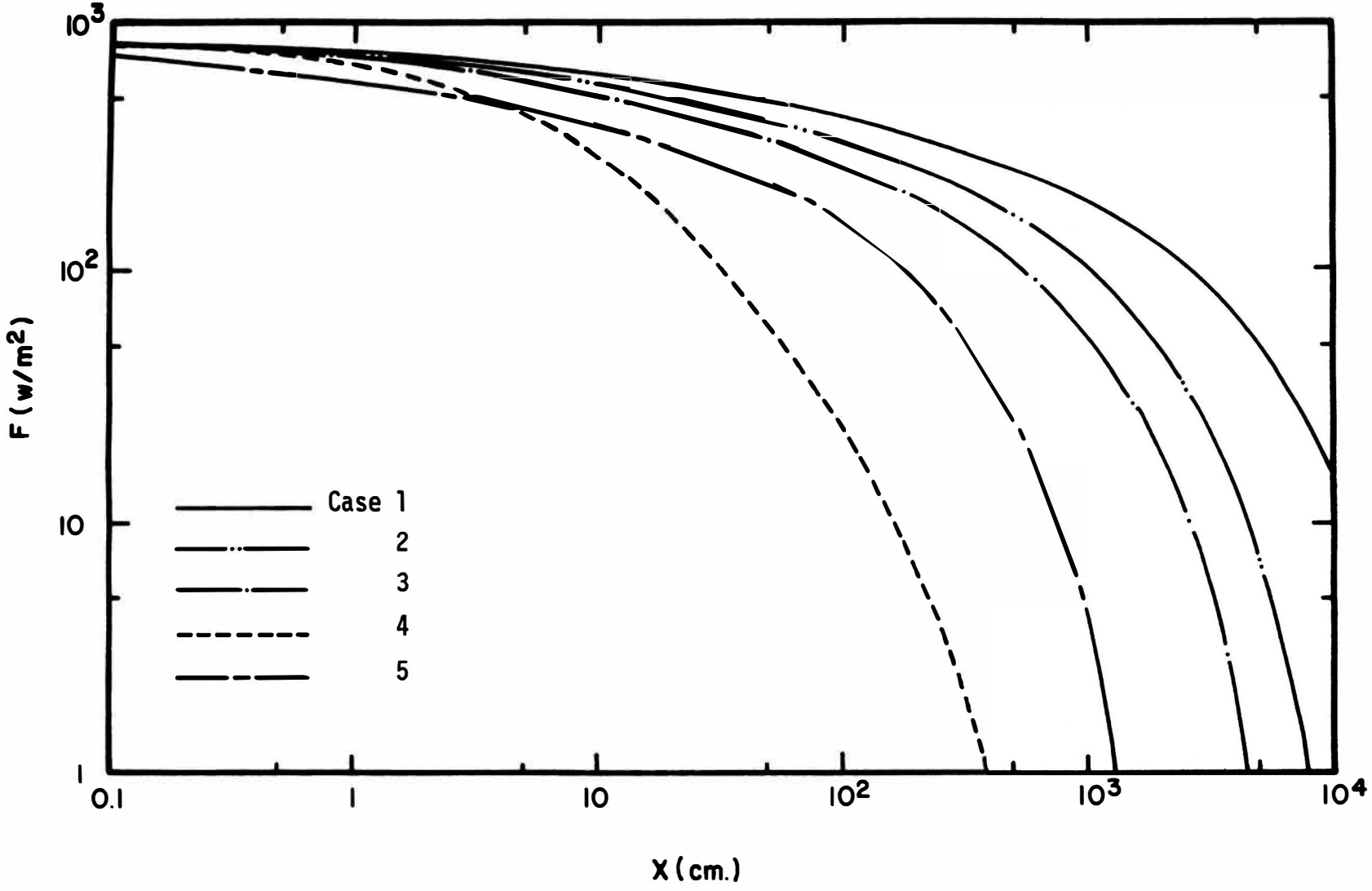

Figure 6. Comparison of Flux Distribution for Normal Incident Solar Radiation

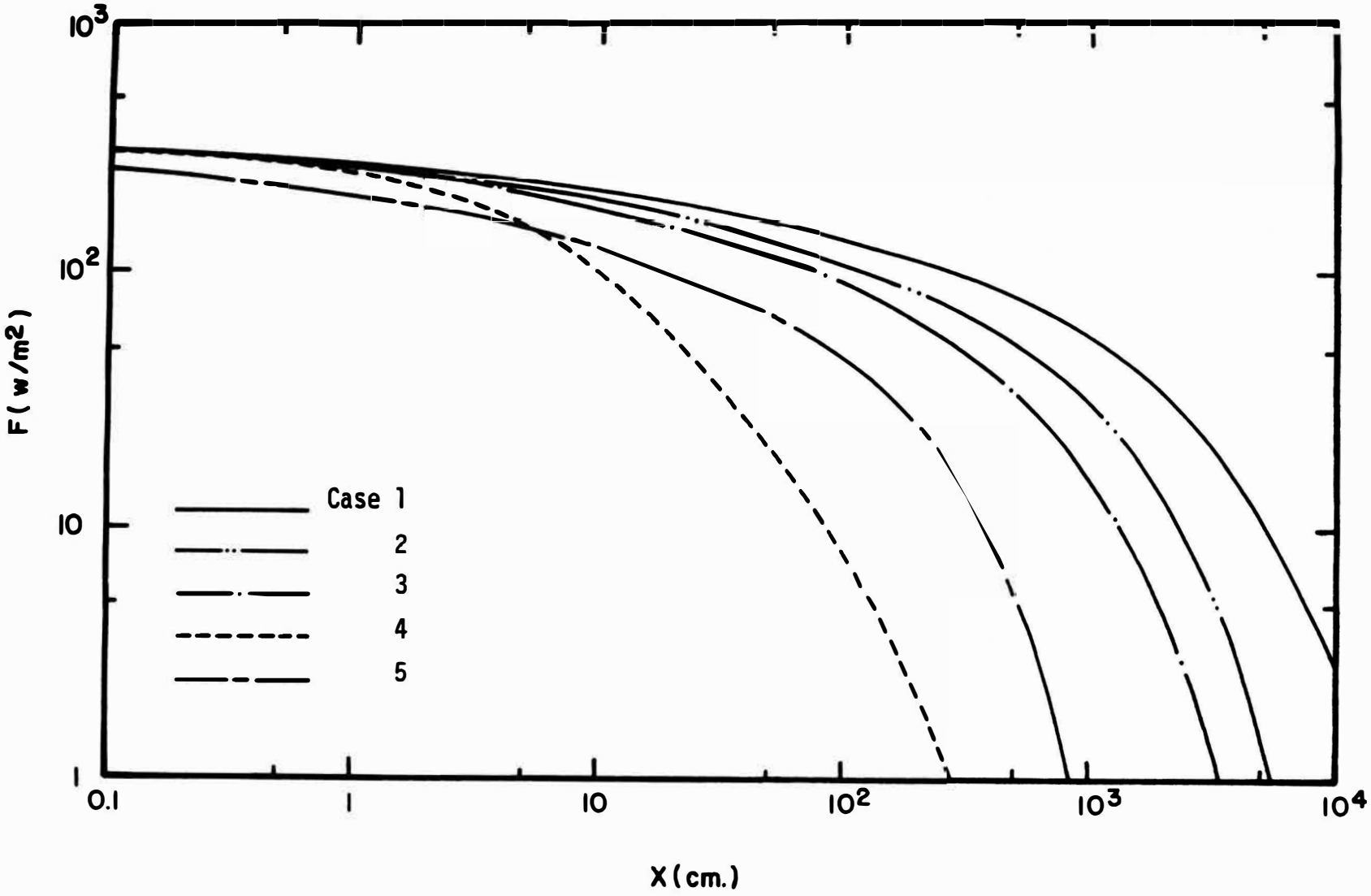

Figure 7. Comparison of Flux Distribution for 60° Incident Solar Radiation

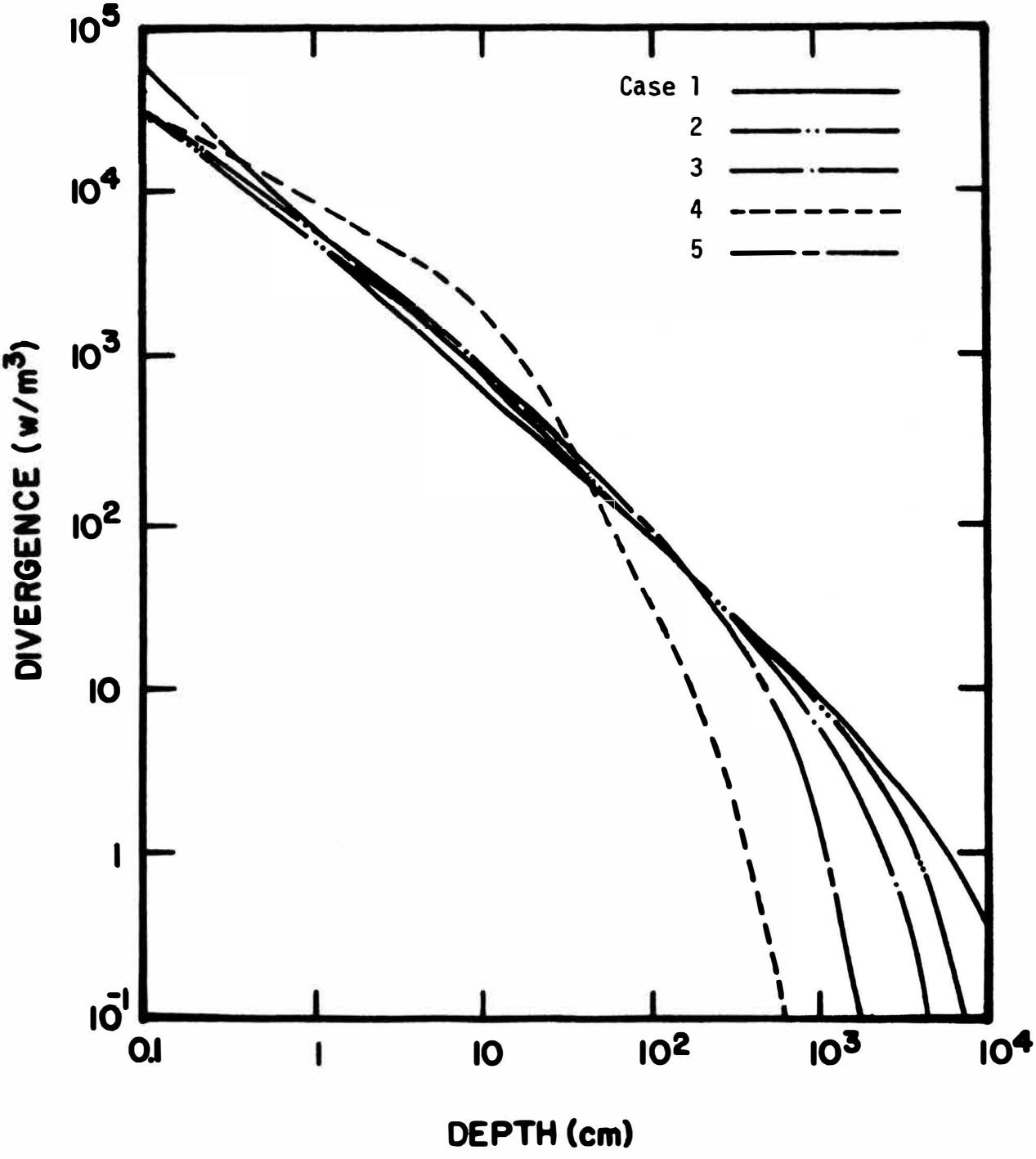

Figure 8. Comparison of the Divergence for Normal Incidence

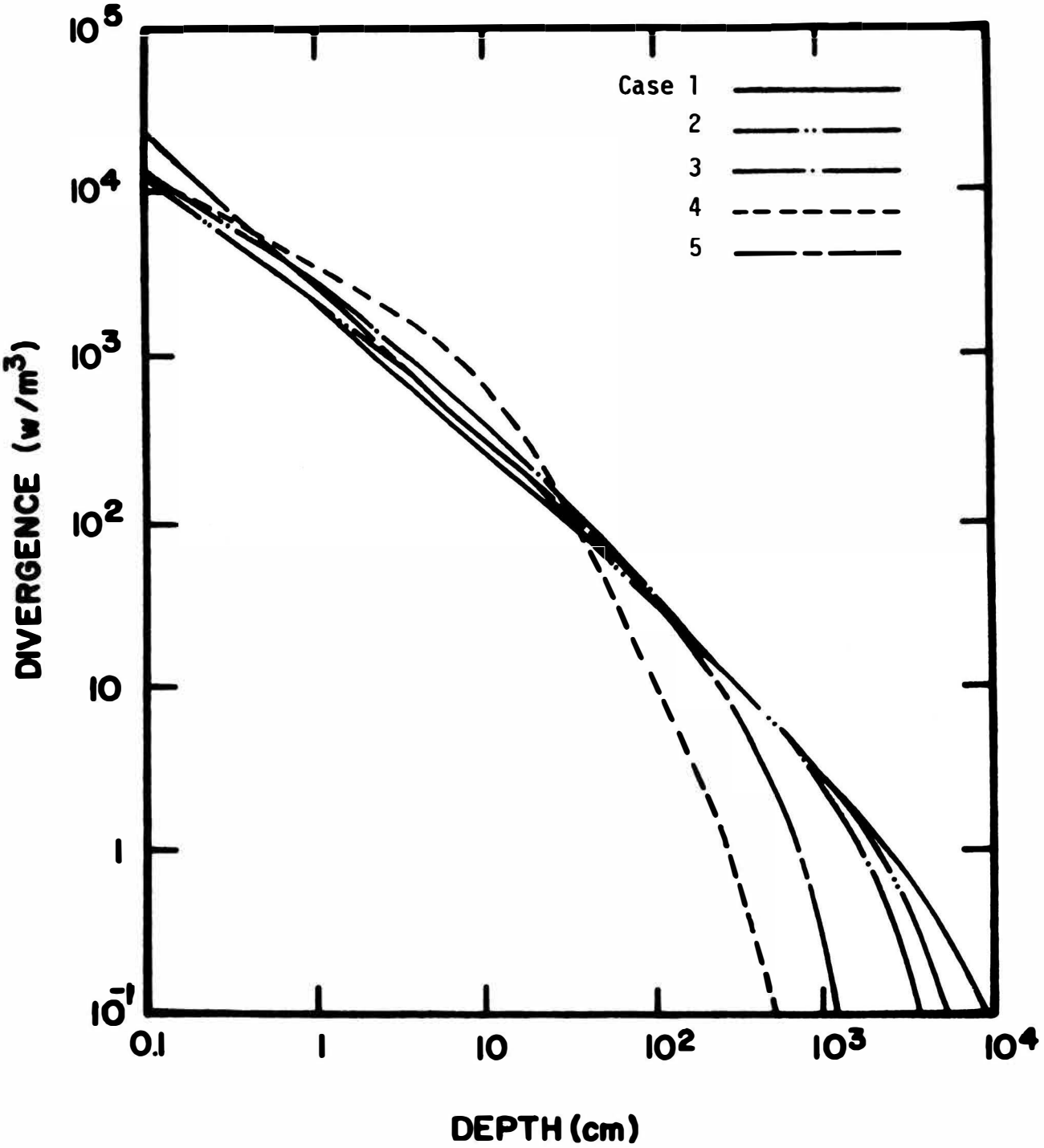

Figure 9. Comparison of the Divergence for 60° Incident Angle

The results indicate only the trend and the effect of the optical properties on the flux distribution. For a more realistic prediction, the monochromatic optical properties of the turbid water needs to be measured at the location of interest.

VII. ENERGY EXCHANGE AT THE AIR-WATER INTERFACE

The energy exchange models at the air-water interface will determine the surface temperature and influence strongly the temperature distribution below the interface. Therefore, it is important that the models do represent realistic natural conditions. As stated in Equation (3), the energy exchange at the interface is due to convection from and to the surface, $F_c(t)$, evaporation from the surface (condensation is neglected), $F_v(t)$, and radiation from and to the surface, $F_{rad}(t)$. The last component consists of diffuse incident radiation absorbed at the surface, $F_d(t)$ and the energy emitted by the water surface, $F_s(t)$. The thermal energy balance at the interface is presented by:

$$q_s(t) = F_c(t) + F_v(t) + F_d(t) + F_s(t) \tag{20}$$

In addition to the above thermal energy terms, a mechanical energy which is due to wind mixing at the surface must also be included as a part of the total energy balance. This term will be treated separately later.

A. CONVECTION

Energy loss or gain by convection at the interface is governed by Newton's law of cooling which is given:

$$F_c(t) = -h_c(t)[T(o,t) - T_a(t)] \tag{21}$$

where h_c is the convective heat transfer coefficient and T(o,t) is the transient surface temperature. Energy leaving the surface is

considered as a negative quantity in our system. The heat transfer coefficient is predicted by relating frictional forces and heat transfer. The heat transfer coefficient is given by [58]

$$h_c(t) = \frac{g_c \tau}{V_a(t)}[C_{pa}(K_a/\mu_a)^2]^{1/3} \tag{22}$$

τ is the shear stress at the surface of the water and is defined for rough water surface by [29]

$$\tau = 1.35 \times 10^{-1} \rho_a V_a(t)^2/g_c \tag{23}$$

where ρ_a is the density, C_{pa} is the specific heat, K_a is the thermal conductivity, μ_a is the absolute viscosity of the air and $V_a(t)$ is the wind speed. The quantity g_c is a dimensionless constant used for consistent units g_c = 1 m kg/n sec^2.

B. EVAPORATION

Energy loss from the surface due to evaporation is one of the major modes of energy transfer. It can be expressed in terms of Ficks law by

$$F_v(t) = -h_m(t)[C_w(t) - C_a(t)]h_{fg} \tag{24}$$

where $h_m(t)$ is the mass transfer coefficient, h_{fg} is the latent heat taken as 2452 KJ/kg and $C_w(t)$ and $C_a(t)$ is the water vapor concentration at the water surface and the ambient air respectively. The heat and mass transfer analogy is used to determine the mass transfer coefficient given by

$$h_m(t) = (h_c(t)/\rho_a C_{pa})(Le)^{-2/3} \tag{25}$$

where Le is the Lewis number and for air-water interface is taken to be 0.845. The water vapor concentrations are calculated using the ideal gas relation

$$C_a(t) = P_a \Psi / R_w [T_a(t) + 273] \tag{26}$$

$$C_w(t) = P_o / R_w [T(o,t) + 273] \tag{27}$$

where P_a and P_o are the partial pressure of the water vapor in the atmosphere and at the water surface respectively, R_w is the gas constant, $T_a(t)$ and $T(o,t)$ are the temperature in degrees Centigrade in the atmosphere and at the interface respectively and Ψ is the relative humidity. The mass transfer due to either condensation or evaporation is neglected and only the energy associated with that process is taken into account in this model.

C. SURFACE RADIATION

Mostly long wave radiant energy is emitted and absorbed at the surface of the water. The atmospheric radiation is considered to be entirely absorbed at the surface and is given by

$$F_d(t) = \varepsilon_a \sigma T_{aK}^4 \tag{28}$$

where the atmospheric emissivity, ε_a, is a function of the ambient temperature in degrees Kelvin, T_{aK}, and it is given by [58]

$$\varepsilon_a = 1 - 0.261 \exp[-7.777 \times 10^{-4} (273 - T_{aK})^2] \quad (29)$$

The water surface may be assumed to emit or lose radiant energy at a rate given by

$$F_s(t) = -\varepsilon_w \sigma [T(o,t) + 273]^4 \quad (30)$$

where ε_w is the total hemispherical water emittance and equal to 0.9 and σ is the Stefan Boltsmann constant. The interface boundary conditions expressed by Equation (3) becomes

$$-K \frac{\partial T}{\partial x}(o,t) = F_v(t) + F_c(t) + F_d(t) + F_s(t) \quad (31)$$

VIII. AMBIENT CONDITIONS

One of the difficulties associated with modeling the stratification development of a reservoir is the inability to describe accurately the transient behaviors of ambient conditions. The models used in this study are described below.

A. AMBIENT TEMPERATURE

Based on measurements in our region, the transient ambient temperature variation in the spring part of the year for Phelps Co. can be expressed by the following equations:

$$T_a(t_s) = 10 + 16.67 \sin \frac{\pi t_s}{2N} \qquad 0 \le t_s \le N \qquad (32)$$

$$T_a(t_s) = 26.67 - 16.67 \sin \frac{\pi(t_s - N)}{2D} \qquad N \le t_s \le 24 \qquad (32a)$$

where t_s is the time from sunrise measured in hours, N and D are the night and day length in hours respectively and $T_a(t)$ is the ambient temperature in degrees Centigrade. Temperatures resulting from this model are presented as Figure 10 with some measured data [61].

B. WIND SPEED

The wind velocity model that will be used in this study has been introduced and used by Hill and Viskanta [25]. It is based on average measured behavior during spring and summer months in Indiana.

$$V_a(t_m) = 3.1 + 0.9[\pi(t_m - 9)/12] \qquad (33)$$

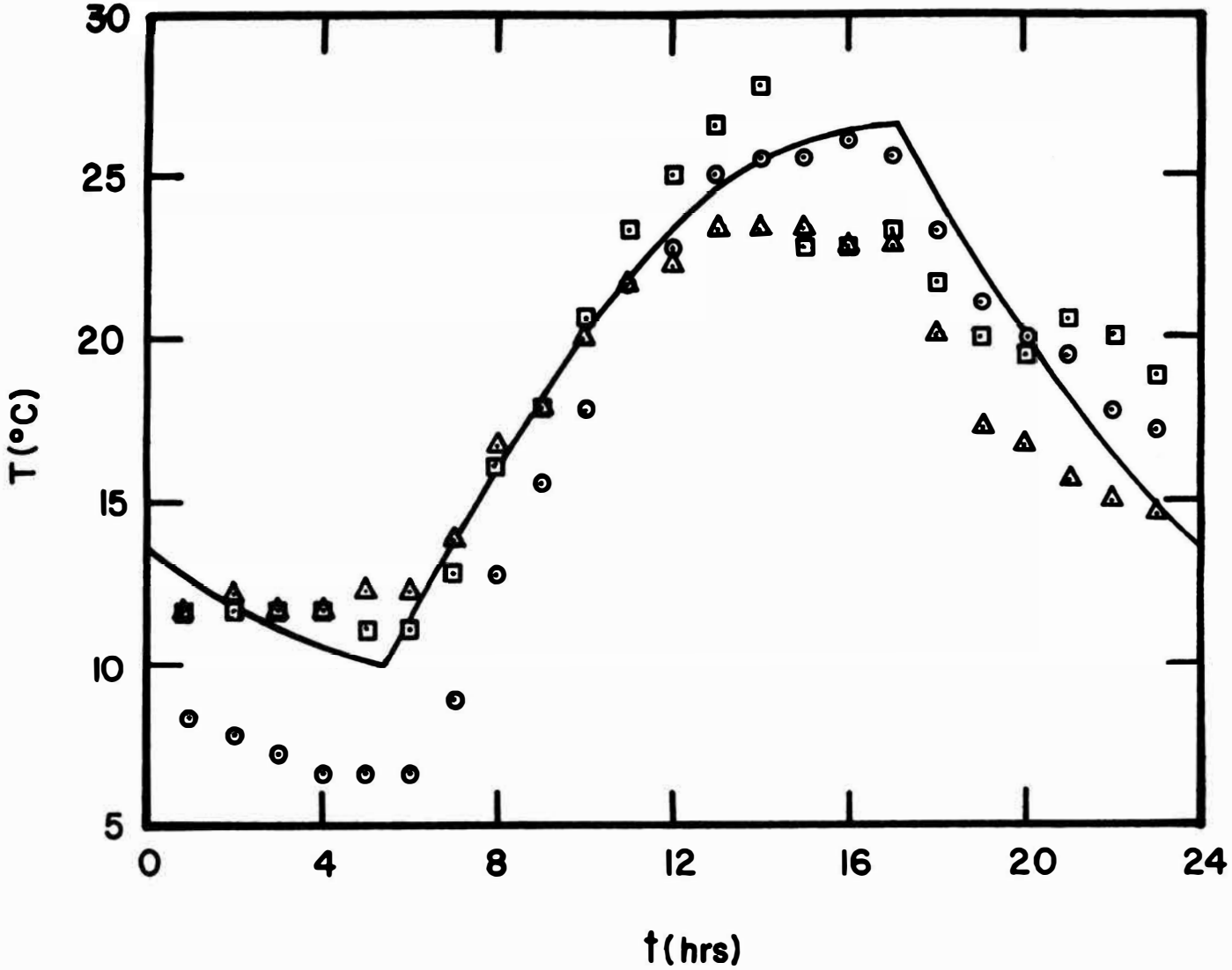

Figure 10. Ambient Temperature Model

where $V_a(t_m)$ is the ambient wind speed in meters per second and t_m is the time measured from midnight in hours. A comparison between the model and data for our region [61] is shown in Figure 11.

C. RELATIVE HUMIDITY

Based on measured data [61] in our region, the relative humidity, Ψ, during the spring time of the year can be modeled by the following equations:

$$\Psi(t_s) = 90 - 40 \sin (\pi t_s/2N) \qquad 0 \leq t_s \leq N \qquad (34)$$

$$\Psi(t_s) = 50 + 40 \sin [\pi(t_s - N)/(2D)] \qquad N \leq t_s \leq 24 \qquad (34a)$$

A comparison with measured data is shown in Figure 12. It is interesting to note that the characteristic variations of ambient temperature and humidity have cycles of the same period but out of phase by half of a period.

Sunrise, sunset, day length, incident angle, and level of the solar load for our local (Phelps Co.) conditions were evaluated through models outlined by Duffie and Beckmann [59].

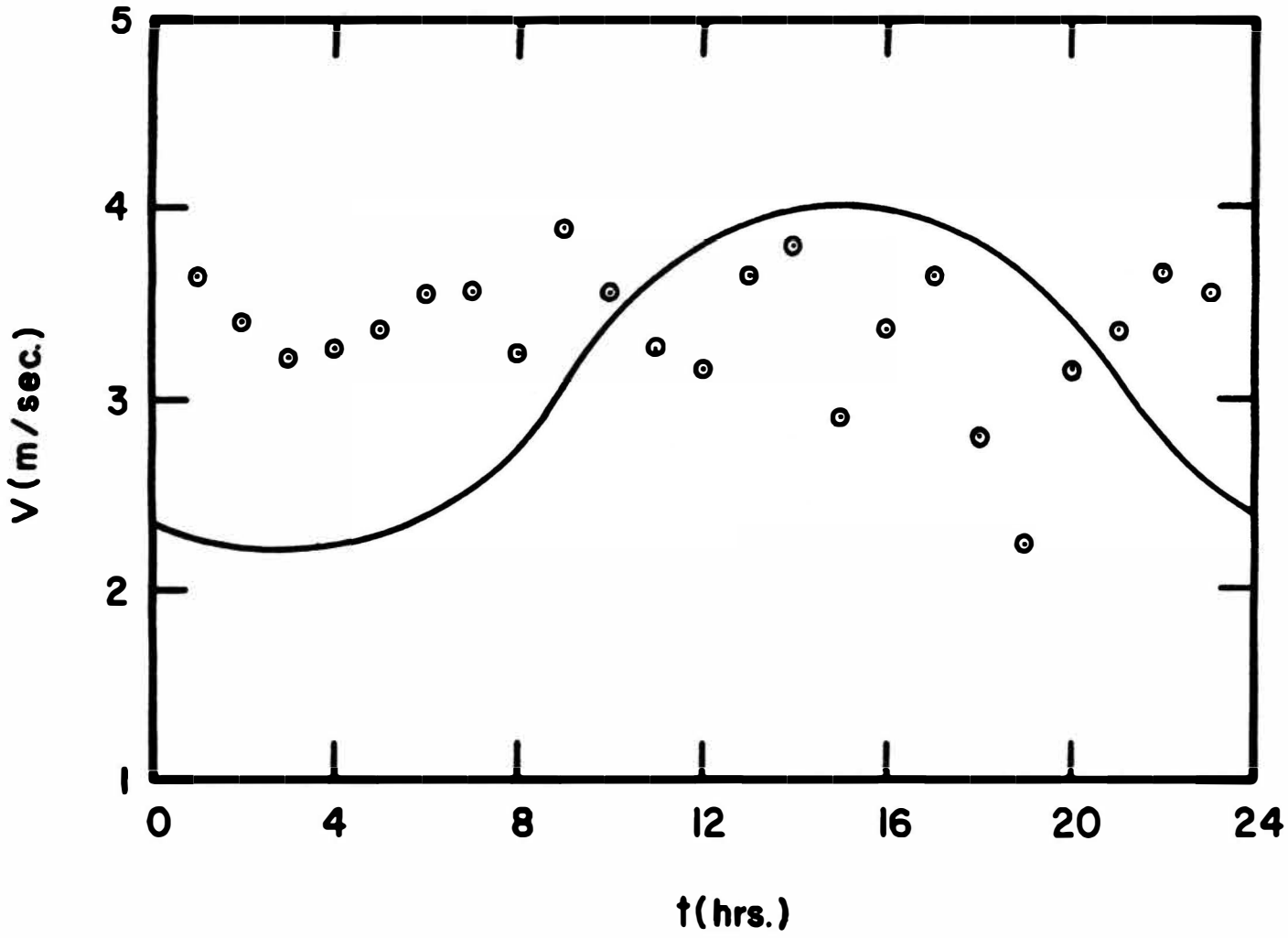

Figure 11. Wind Speed Model

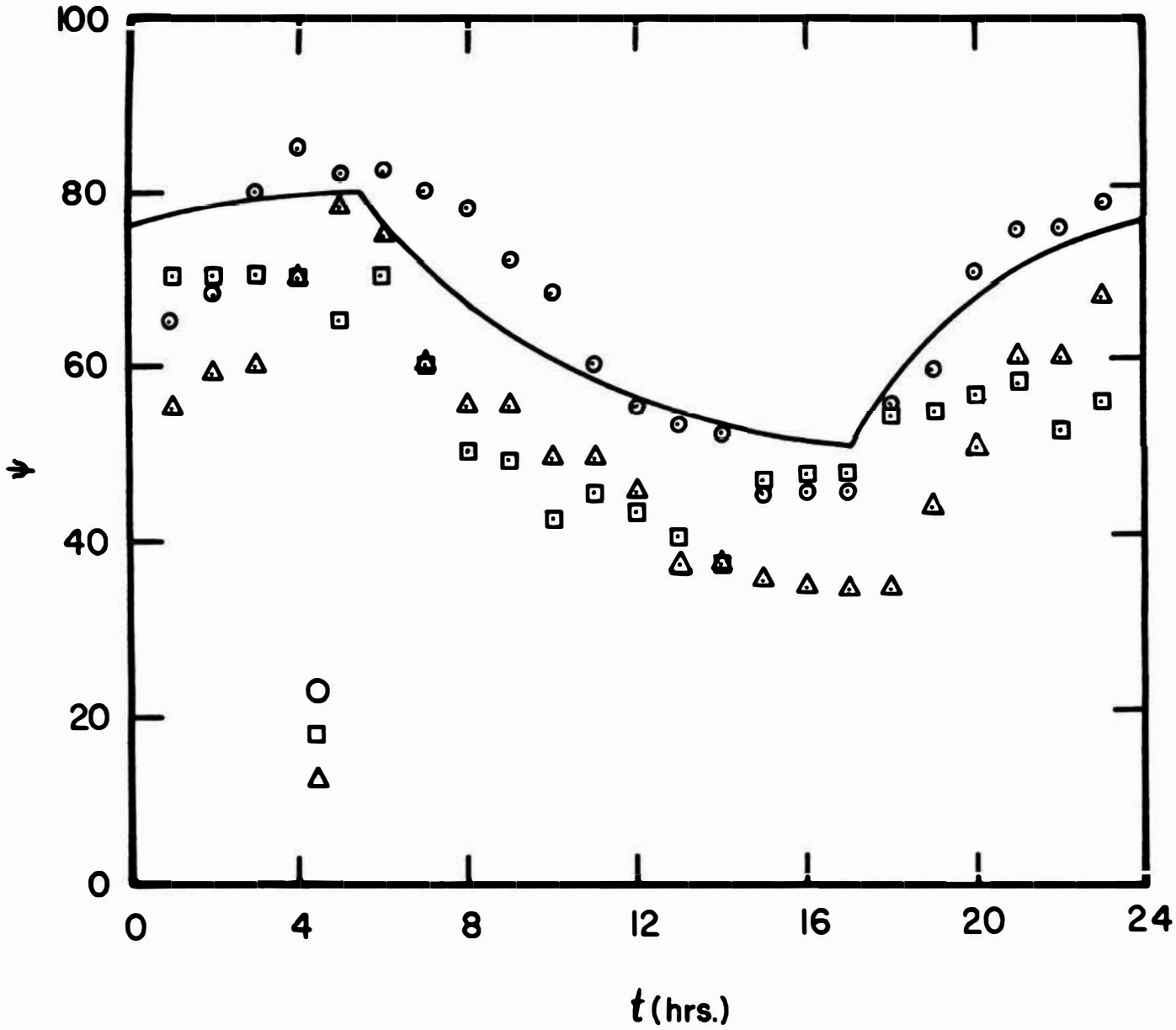

Figure 12. Relative Humidity Model

IX. FINITE DIFFERENCE SOLUTION

The numerical solution of the energy equation, Equation (1), with the initial boundary conditions as expressed by Equations (2), (4) and (31) respectively was obtained using explicit finite difference method. The finite difference equations governing the solution are given below. The temperature at the surface is given by

$$T(o,t+\Delta t) = \frac{2\alpha\Delta t}{\Delta x^2}\left[T(\Delta x,t) + \frac{\Delta x}{K} q_s(t)\right] + T(o,t)\left[1 - \frac{2\alpha\Delta t}{\Delta x^2}\right] - \frac{\Delta t}{\rho C} H(o,t) \tag{35}$$

where $q_s(t)$ is the surface energy loss given by Equation (20). The temperature within the medium is given by

$$T(x,t+\Delta t) = \frac{\alpha\Delta t}{\Delta x^2}\left[T(x+\Delta x,t) + T(x-\Delta x,t)\right] + T(x,t)\left[1 - \frac{2\alpha\Delta t}{\Delta x^2}\right] - \frac{\Delta t}{\rho C} H(x,t) \tag{36}$$

At the point where the node distance changes from Δx to Δx_1 the temperature is given by

$$T(x,t+\Delta t) = \frac{2\alpha\Delta t}{\Delta x(\Delta x + \Delta x_1)}\left[T(x+\Delta x_1,t)\frac{\Delta x}{\Delta x_1} + T(x-\Delta x,t)\right] + T(x,t)\left[1 - \frac{2\alpha\Delta t}{\Delta x\Delta x_1}\right] - \frac{\Delta t}{\rho C} H(x,t) \tag{37}$$

The resulting finite difference solution accounts for the energy added to the interface by the wind shear forces. To account properly for this additional mode of energy transfer, the velocity distribution needs to be examined through the momentum equations and additional terms should be included in the energy equation to describe this physical phenomenon. The mixing motion which results from the wind action on the interface plays a major role in distributing the energy through the reservoir and it will affect its stratification structure. The exact treatment of that affect is, however, beyond the scope of this study and will be accounted for through an approximate but physically realistic model.

Most of the methods used to date for predicting stratification development in lakes or reservoirs, either ignored the effect of wind or included that effect indirectly through the use of selected turbulent diffusion coefficient. That method has the disadvantage that time and depth variable diffusivity must be selected or derived from measured flow and temperature distribution. Stefan and Ford [40] introduced a method, which will be used in this study, that accounts for wind energy input in a more direct fashion. Turbulence obtained from wind acting on the water surface or from convection due to unstable buoyancy gradients will result in complete isothermal mixing of the upper strata to a level called "Mixing Depth". The temperature and the depth of the mixed layer is predicted by making a balance between the energy of stirring induced by the wind and the change in potential energy induced by buoyant forces.

A discrete element approach which is used in the finite difference calculations of the temperature distribution was also used to determine the mixing depth. The energy input to the surface by the wind during a time period Δt is given by

$$E_k = \tau V^* A_s \Delta t \tag{38}$$

where V^* is the shear velocity on the water side of the interface, τ is the shear stress and A_s is the surface area. Since shear stress is constant across the interface, the shear velocities are related [60] by

$$V^* = (\rho_a/\rho)^{1/2} U^* \approx 0.035 U^* \tag{39}$$

ρ_a and ρ are the densities of the air and the water respectively and U^* is the shear velocity at the air side of the interface. Wu [41] expressed the shear stress and shear velocities in terms of a shear stress coefficient, C, which is a function of both wind speed, U, and surface roughness. The shear velocity is given by

$$U^{*2} = CU^2 \tag{40}$$

and the shear stress is given by

$$\tau = C\rho_a U^2 \tag{41}$$

For wind speeds below 15 meters/sec, the stress coefficient is given by

$$C = 5 \times 10^{-4} U^{1/2} \tag{42}$$

Utilizing the above equations, the energy input, as expressed by Equation (37), can be expressed by

$$E_k = 0.035 \rho_a C^{3/2} U^3 A_s \Delta t \tag{43}$$

The density is in Kg/m^3, A_s in meters, Δt in seconds, U in meters per seconds and C is dimensionless. The resulting energy is in Newtons-meters.

The potential (buoyant) energy deficit of the mixed isothermal layer relative to a layer immediately below it can be evaluated from

$$E_p = g \sum_{i=1}^{m} A(i,K) \Delta z_i [\rho(m+1,K) - \rho(i,K)] \sum_{j=i}^{m} \Delta z_j \tag{44}$$

g is the acceleration of gravity equivalent to 9.8 m/sec^2, Δz_i is the thickness of the individual layers (elements) in meters, $\rho(m+1,K)$ and $\rho(i,K)$ are the densities of the m+1 element and the i^{th} element in kg/m^3 at time K and A(i,K) is the area of the i^{th} element at time K. If the mixed layer of thickness $L = \sum_{i=1}^{m} \Delta z_i$ entrains another element Δz_{m+1}, the thickness of the new mixed layer becomes $L_1 = \sum_{i=1}^{m+1} \Delta z_i$. The entrainment of the new element will usually change the bulk density and the temperature of the mixed layer as well as its potential energy.

The critical condition for wind induced mixing, has been discussed in detail by Stefan and Ford [40] and stated in terms of the

energy ratio $(E_k/E_p) = 1$. If $E_k < E_p$, the thickness of the mixed layer is not varied. If $E_k > E_p$, the thickness of the mixed layer is increased by an element. As a result of this entrainment, the density, temperature and potential energy of the mixed layer changes. This process is continued until the critical energy ratio is reached and mixing ends. At every time increment during the finite difference scheme, the decision of mixing and no mixing is decided by evaluating the energy ratio and comparing it to the critical ratio of 1.

The finite difference solution of the governing equation was performed on an IBM 370/168 digital computer. To satisfy the stability and the convergence criteria [26], the time increments were selected as $t = 0.04$ hours and node distances were varied with depth as follows, $\Delta x = 0.00762$ meters for $0 \leq x \leq 0.03048$, $\Delta x = 0.03048$ meters for $0.03048 \leq x \leq 0.3048$ and $\Delta x = 0.3048$ meters for $x \geq 0.3048$.

To study the effect of changing Δx, on the convergence and stability criteria of the solution, case 4 which is the highly absorbing medium was selected. This case will exhibit the most stringent convergence criteria because its divergence at $x = 0$ is the largest one. The elements, Δx's, in the surface layer (0-0.3 meters) were changed to 0.003 meters and to 0.015 meters in comparison to the ones used for the results which were $\Delta x = 0.0076$ meters. The simulation was carried for a period of ten days and a comparison of the significant results are presented in Figure 13 and Figure 14. It can be seen from Figure 13, that surface temperature at 2 p.m. indicate differences of 4 and 2 degrees for the different sizes of Δx, which indicates that convergence has not been achieved. It should be noted,

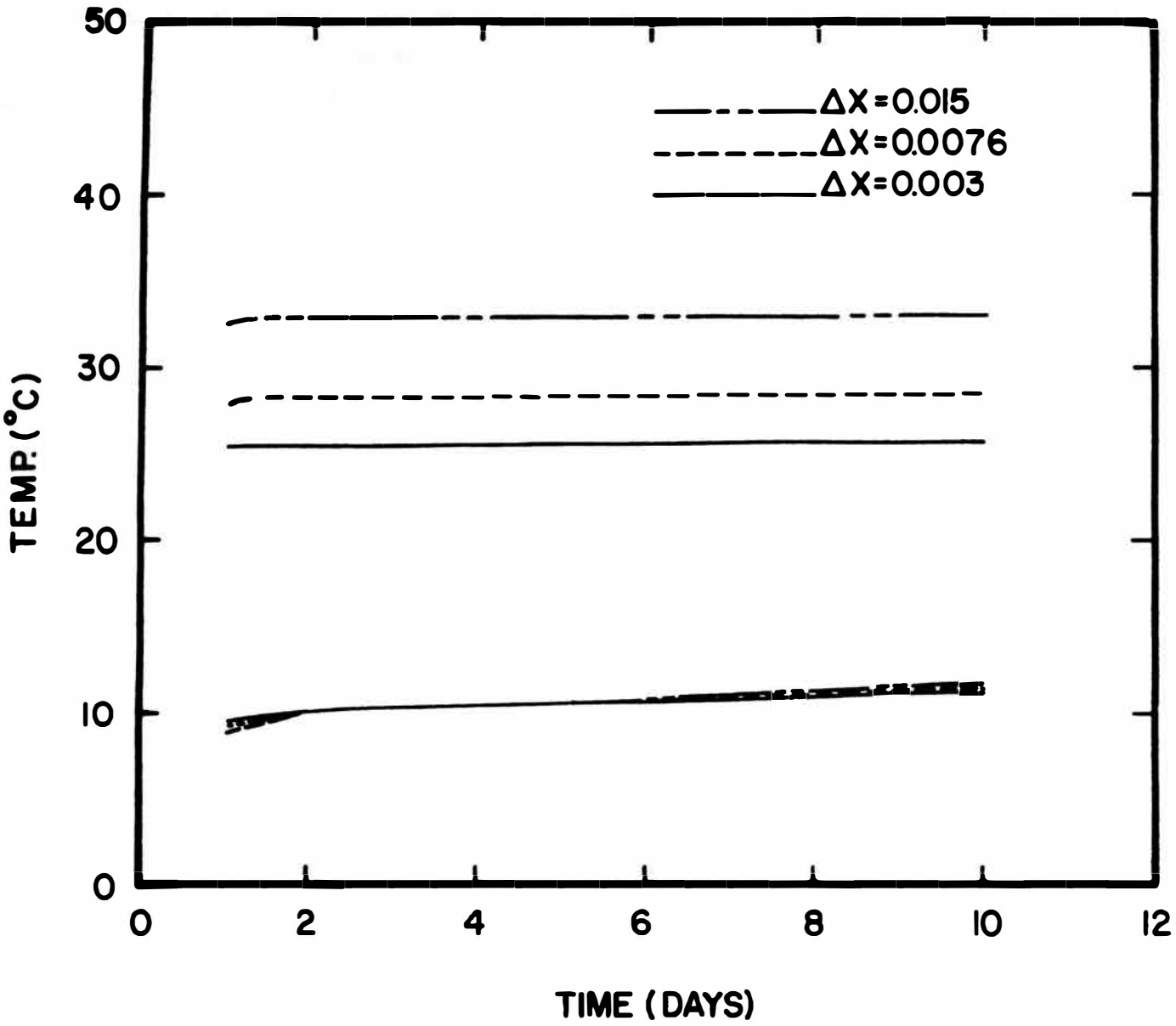

Figure 13. Comparison of Temp Development for Various Δx's

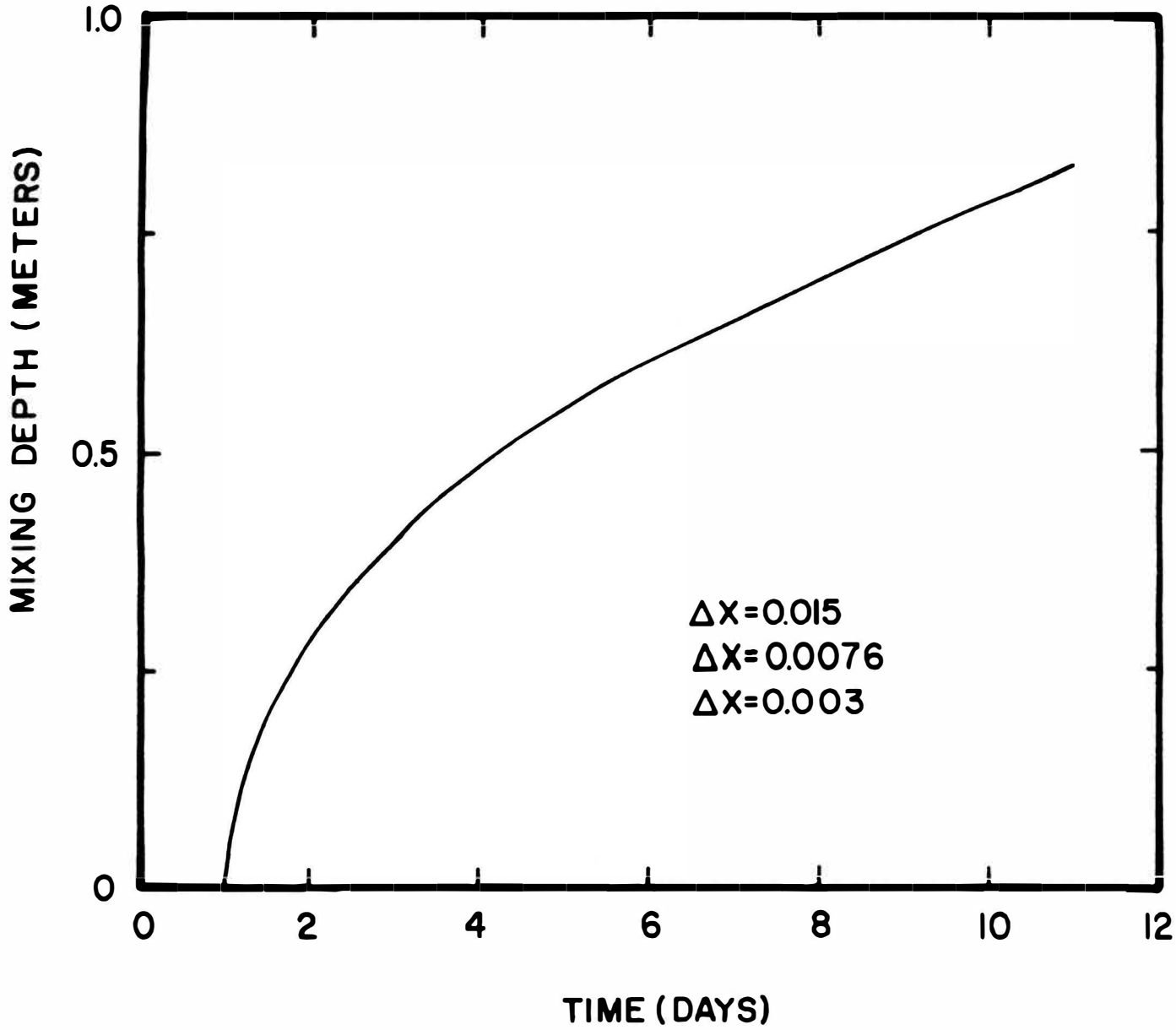

Figure 14. Comparison of Mixing Depth for Various Δx's

however, that for that time of the day differences between the three cases existed only in the upper 0.02 meters of the medium. Below that level the three cases predicted the same development.

If on the other hand, surface temperature at 6 a.m. and the mixing depth are used as the criteria for convergence, it is clear from these figures that convergence has been reached. Obviously the smallest Δx will generate a more accurate profile throughout the simulation period. Indeed there are no mathematical difficulties that are associated with using a smaller Δx. There is, however, an economical consideration associated with the computer time required for simulation. When $x = 0.003$ meters, the time increment must be set at $\Delta t \leq 0.008$ hrs to maintain stability. This adjustment ($\Delta x = 0.0076$ meters to $\Delta x = 0.003$ meters) increases the simulation time for ten days by a factor of 9 (from 2.8 min of CPU to 25 min of CPU).

Since our objective is to simulate stratification development over a long period of time (months) and not the hourly fluctuation of surface temperature, the choice of $\Delta x = 0.0076$ is justified. In addition, one should be aware that in natural situation wave mixing, which is not included in our model, will stir the upper layer and eliminate the high gradients appearing close to the surface at noon. For that reason mean surface temperatures should not be considered as representing natural conditions and should not be used as the criterion for convergence.

X. RESULTS AND DISCUSSION

The ambient conditions described in the previous models were used with the finite difference solution of the energy equation to determine the influence of increased scattering or absorption on the stratification development of deep water impoundment. The initial temperature of the impoundment was taken as uniform at 44°F (6.66°C) simulating early spring conditions for Phelps Co. The simulation was performed for one month period without changing the daily behavior of the solar load or the ambient conditions. Conditions simulating the month of April were selected using Duffie and Beckmann's models [59], sunrise at 5:35 a.m., sunset at 6:65 p.m. were determined making the day length 12.27 hours. Results are presented for Case 1 (non-scattering), Case 3 (lake benson), Case 4 (highly scattering) and Case 5 (highly absorbing) medium.

Surface temperature variations as it develops during the first month of the stratification process is shown in Figures 15 through 17. Figures 15 and 16 present the daily temperature at 6 a.m. and 2 p.m. respectively. They represent approximately the maximum and the minimum temperatures of each day. It is clear from these figures that the surface temperature at 2 p.m. is higher for the more turbid cases while the 6 a.m. value becomes almost independent of the turbidity level of the water. The 2 p.m. value does not change after the fourth day of simulation while the surface temperature at 6 a.m. continues to increase (but at a decreasing rate) throughout the simulation period. The higher surface temperature, which is associated with the higher extinction coefficient, causes a larger energy loss

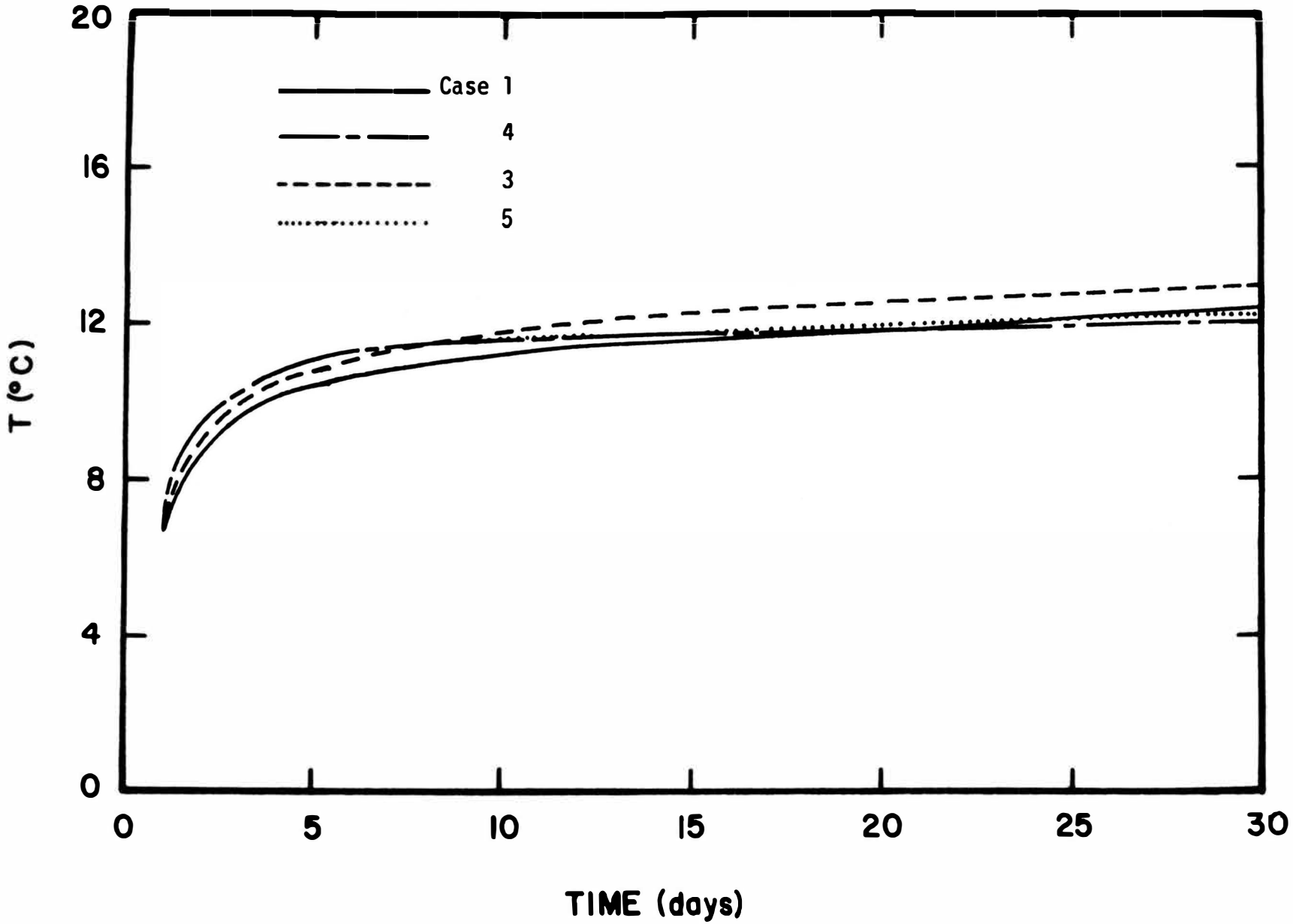

Figure 15. Surface Temperature at 6 a.m.

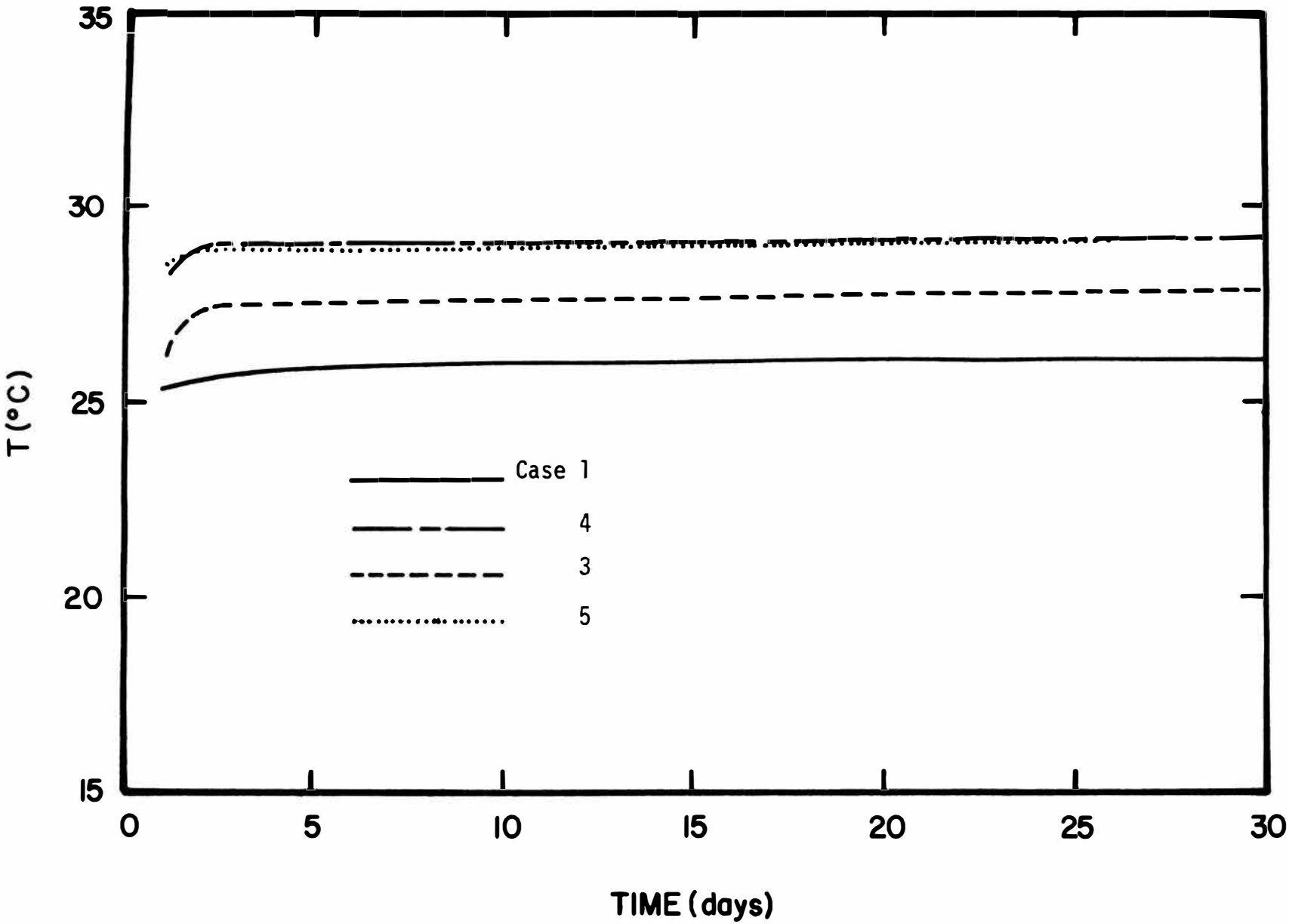

Figure 16. Surface Temperature at 2 p.m.

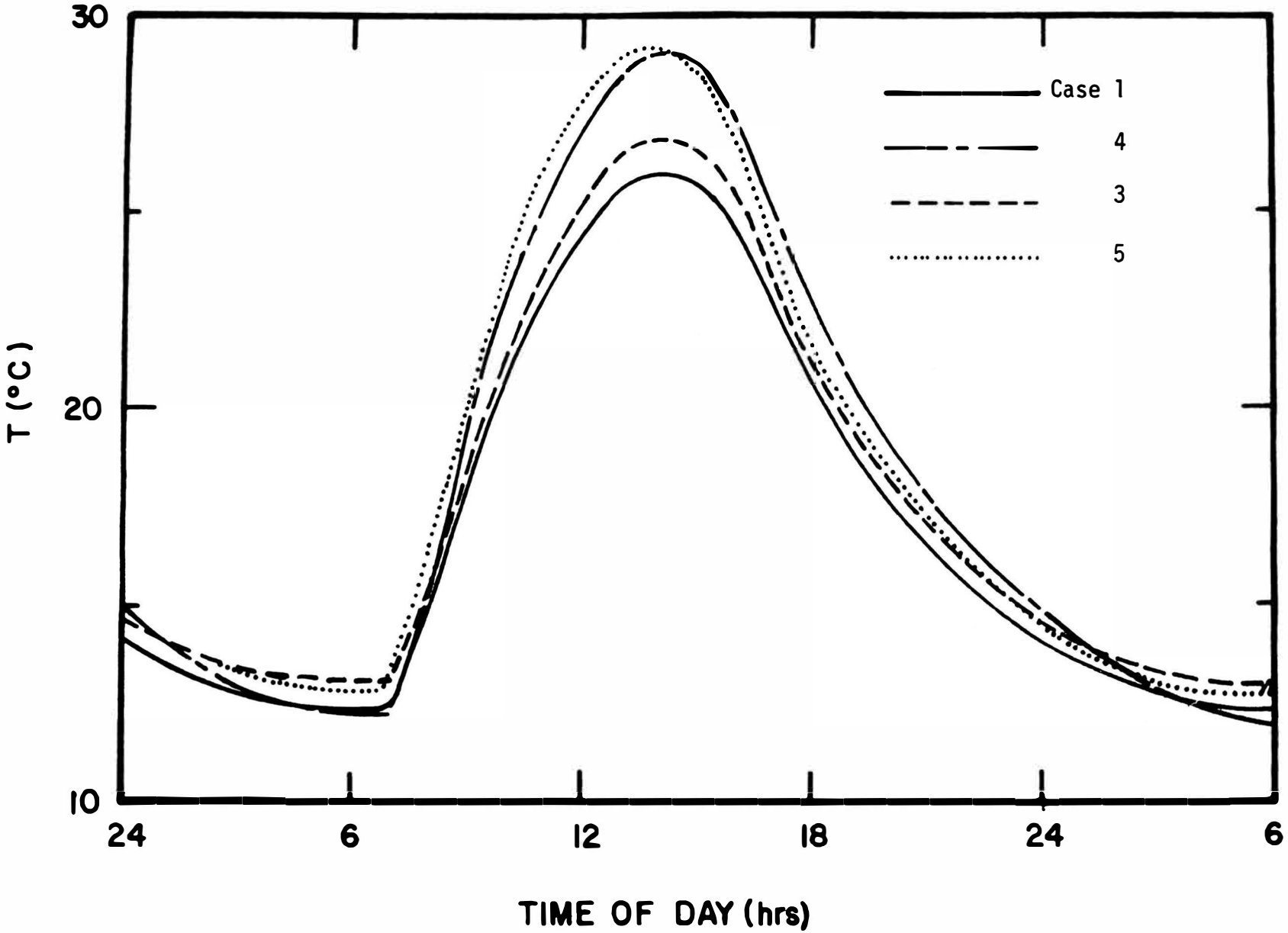

Figure 17. Daily Variations of Surface Temperature, 30th Day

to the surroundings by convection and radiation during the cooling period of the day (from 2 p.m. to 6 a.m.). Since these processes are independent of the turbidity levels of the water they cause the surface temperature at 6 a.m. to be also almost independent of that parameter. The hourly variation of the surface temperature is presented in Figure 17 for the 30th day of the simulation. In all of the water cases the surface temperature was higher than the ambient temperature at 2 p.m. and lower than the ambient temperature at 6 a.m.

The development of these surface temperature profiles seems to indicate an eventual convergence that is a function of the prescribed ambient conditions. Figure 17 represents roughly the equilibrium surface temperature resulting from the present simulation model. It should be emphasized, that the natural behavior does not vary in a cyclic manner day after day as modeled, but will actually change from one day to another in an unpredictable fashion. This will cause the surface temperature to continuously vary in accordance with the existing ambient conditions. In addition, the first few days of this simulation exposes the water to strange ambient conditions that do not match with its thermal status and thus should not be considered as natural behavior. The simulation shows the influence of turbidity on the stratification development.

Temperature distributions through the impoundment during the 30th day of the simulation at both 2 p.m. and 6 a.m., are shown in Figures 18 and 19. They demonstrate the cyclic behavior experienced by the upper water layer. When the extinction coefficient is small, the solar radiation penetrates to very large depths and causes the

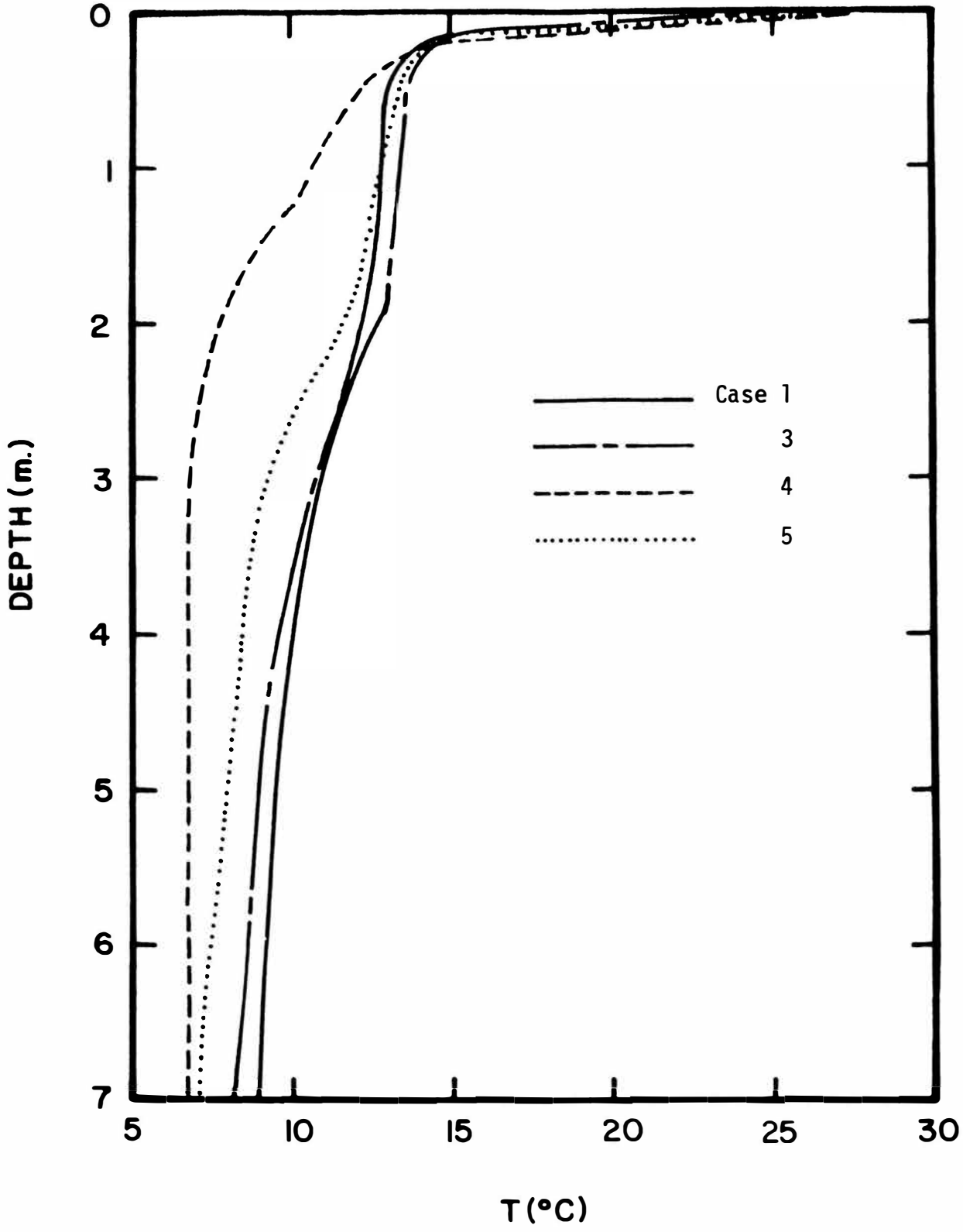

Figure 18. Temperature Distribution at 2 p.m., 30th Day

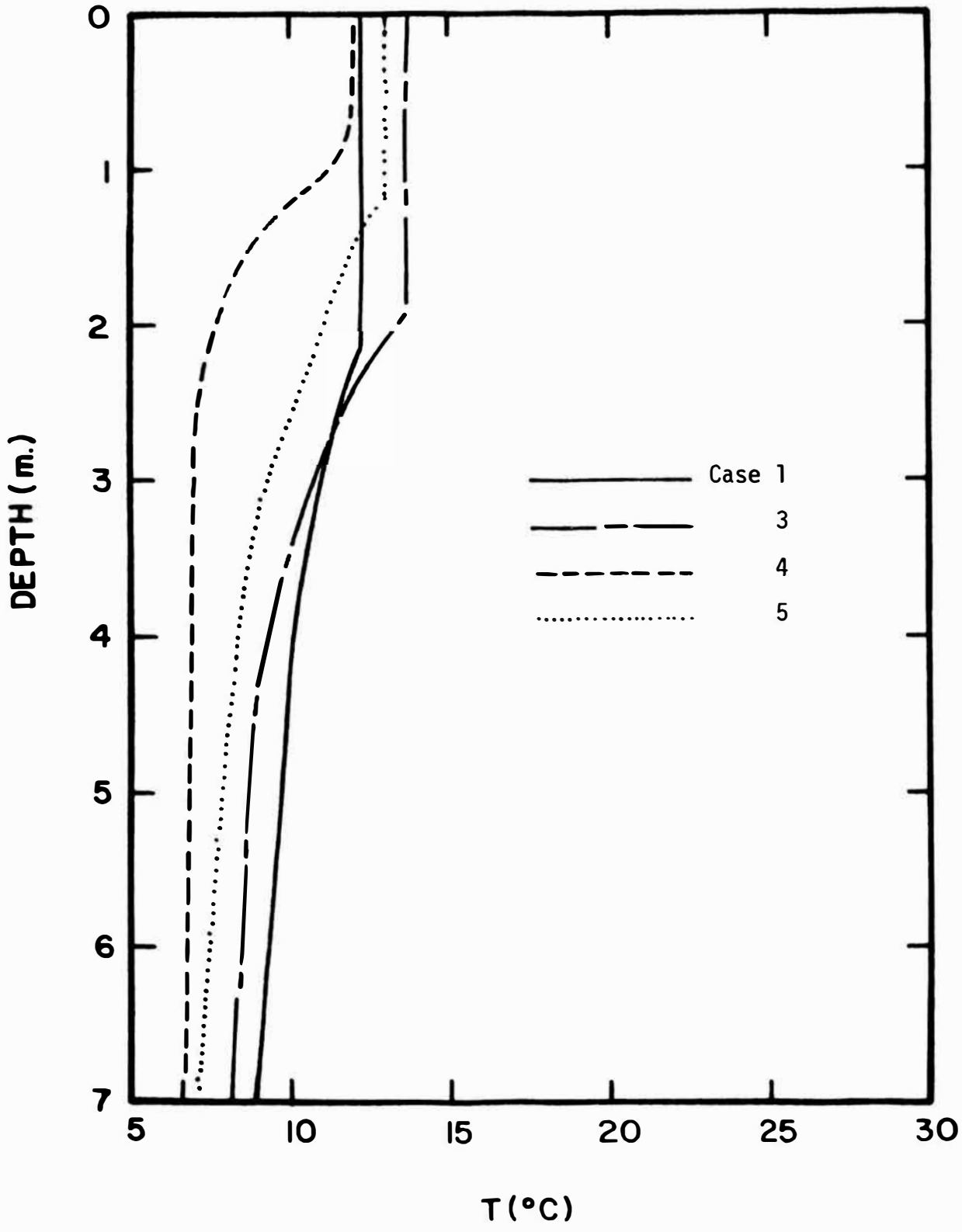

Figure 19. Temperature Distribution at 6 a.m., 30th Day

temperature there to increase. The region which is affected by the solar radiation (affected region) is shown in Figure 20 and as expected it is a strong function of the turbidity level of the water. For the non-scattering case (Case 1), that region reaches 10 meters in fourteen days while for Case 4 (the highly turbid case) it is less than 2 meters. The daily cycle of heating and cooling plus the wind mixing cause the upper layers of the water to mix daily. The development of this mixing depth is shown as Figure 21. Similar to the affected region, the mixing depth depends strongly on the turbidity levels of the water. This depth continues to increase beyond the 30th day of simulation. The magnitudes of the energy transfer components at the interface are presented as Figure 22. The emission and the absorption of radiation at the surface represent the major components and they are opposite in direction. The convection and evaporation components are of the same order of magnitudes.

The above results indicate that the turbidity level of the water will affect the surface temperature during the heating part of the day and its affect diminishes during the cooling part of the day. The turbidity levels has significant influence on the stratification development (turbid water will stratify sooner and shallower) because it affects both the mixing depth and the affected region. These two parameters are still developing beyond the 30th day of simulation while the surface temperature appears to have reached equilibrium level. The trends of the predicted results are similar to observed natural behavior.

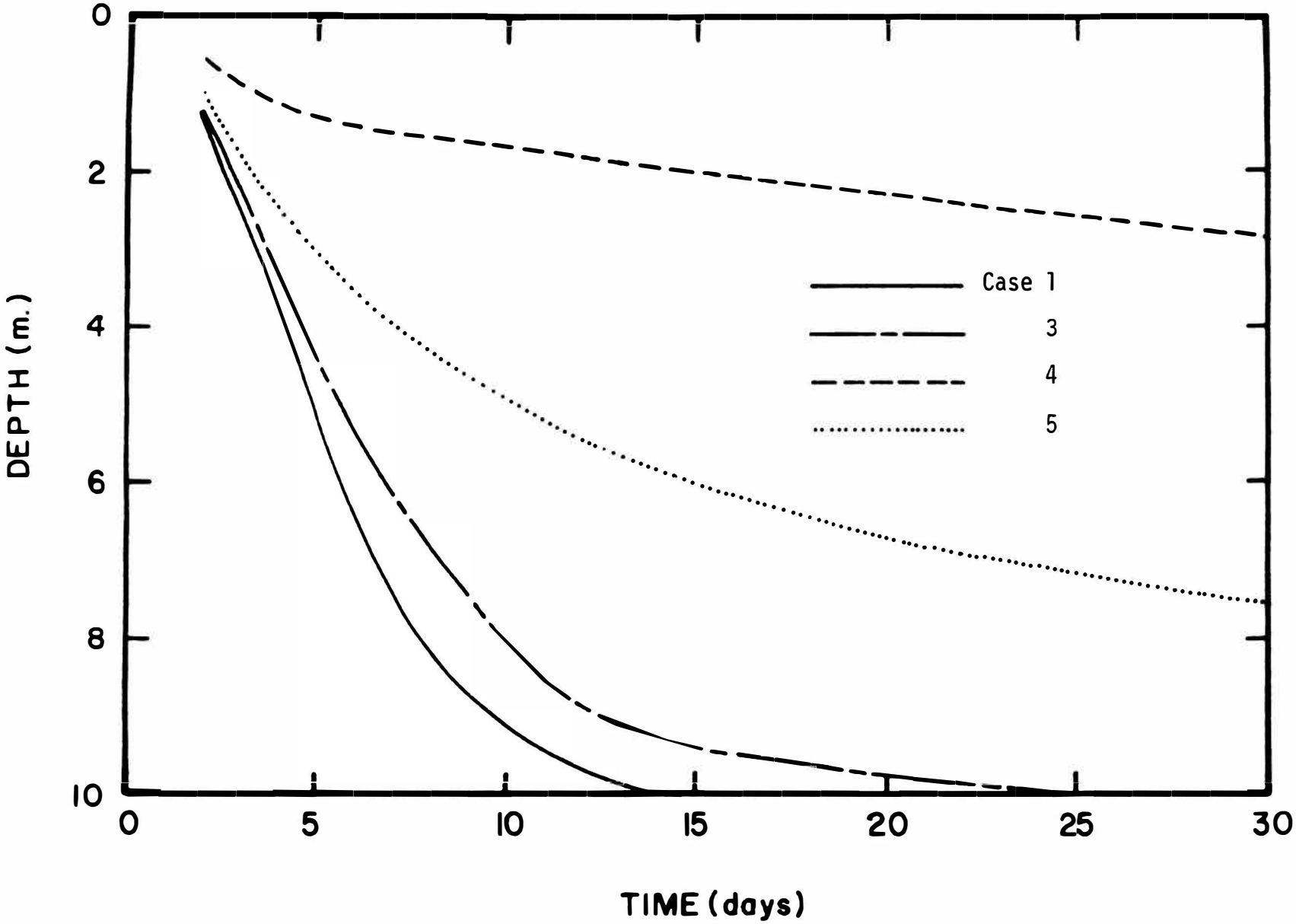

Figure 20. Development of the Affected Region

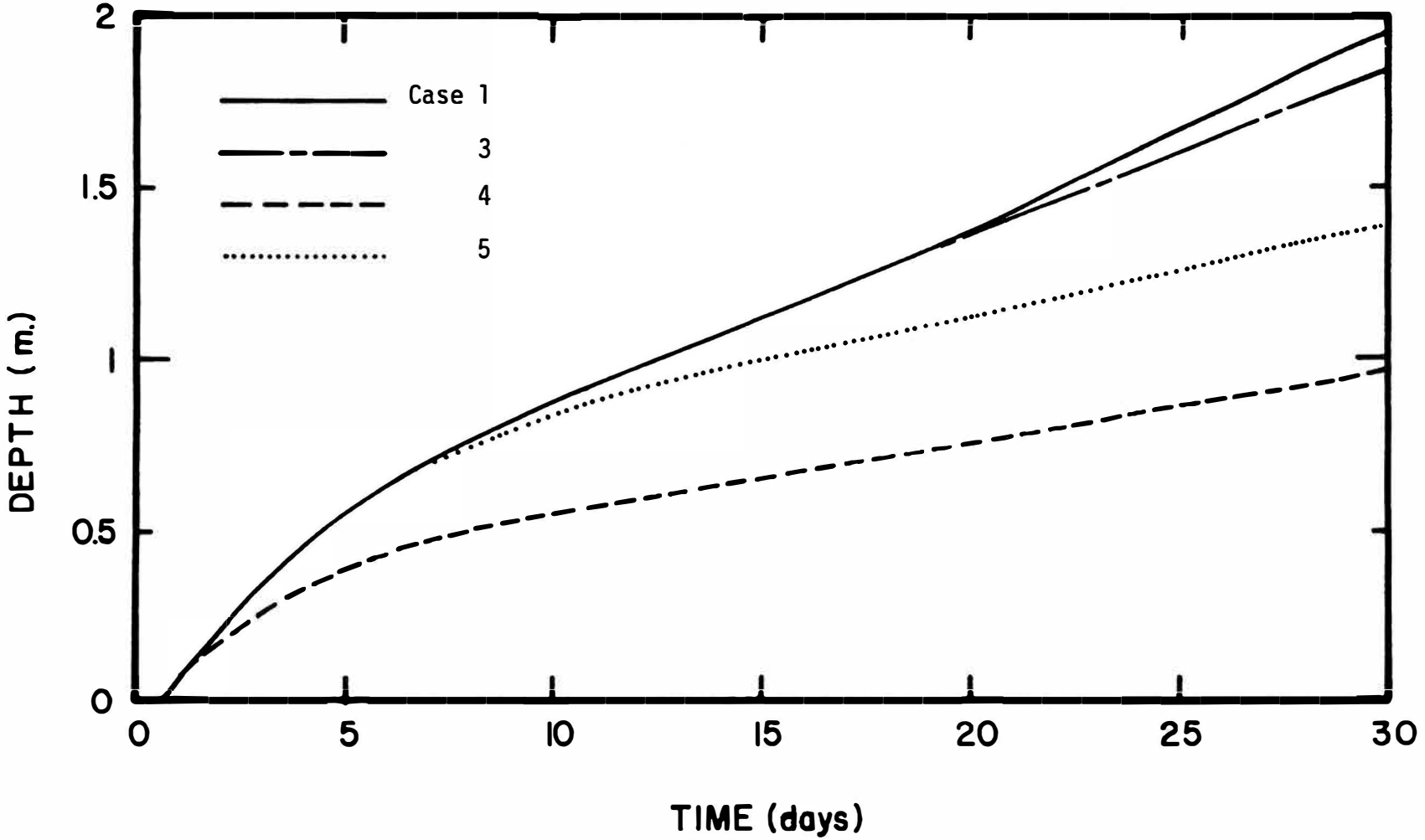

Figure 21. Development of Mixing Depth

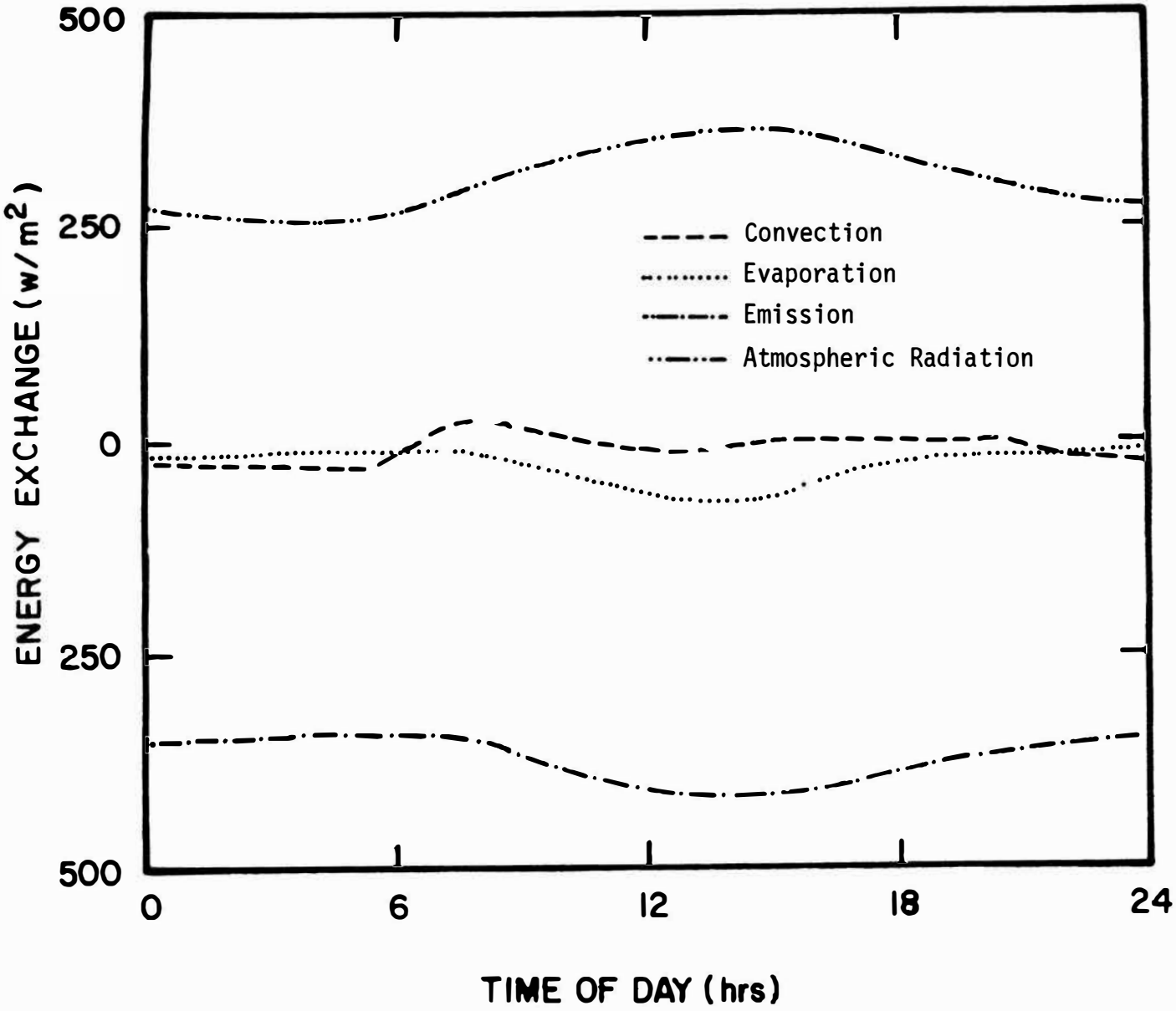

Figure 22. Surface Heat Transfer for Case 3 and 30th Day

XI. CONCLUSIONS AND RECOMMENDATIONS

The results of this study indicate that turbidity is an important parameter in the stratification development of water reservoirs. Its influence is felt primarily in the development of the thermocline depth and not in the surface water temperature, which appears to be a function of ambient conditions. Very turbid water causes the thermocline to be established more quickly, and causes thermoclines to develop at a lesser depth than the less turbid cases.

The next steps for the continuation of this study are the investigation of the effect of turbulent diffusivity, to determine whether this will aleviate the problem of an afternoon temperature spike; and the generation of fluxes with appropriate boundary conditions to model behavior in a finite media.

BIBLIOGRAPHY

1. Rabinowitch, E., and Govinedjee, Photosynthesis, John Wiley & Sons, Inc., New York, 1969.

2. Odum, E.P., Fundamentals of Ecology, Third Edition, W.B. Saunders Company, Philadelphia, 1971.

3. Kormondy, E.J., Concepts of Ecology, Prentice-Hall Inc., Englewood Cliffs, New Jersey, 1969.

4. Moss, D.N., "Solar Energy in Photosynthesis," Solar Energy, Vol. 11, No. 3, 1967.

5. Strickland, J.D.H., "Solar Radiation Penetrating the Ocean. A Review of Requirements, Data, and Methods of Measurement, with Particular Reference to Photosynthetic Productivity," Journal of Fisheries Research Board of Canada, Vol. 15, No. 3, 453-493, 1958.

6. Ryther, J.H., "Photosynthesis in the Ocean as a Function of Light Intensity," Limnology and Oceanography, Vol. 1, No. 1, 61-70, 1956.

7. Fee, E.J., "A Numerical Model for the Estimation of Photosynthesic Production, Integrated Over Time and Depth, In Natural Waters," Limnology and Oceanography, Vol. 14, No. 6, 906-911, 1969.

8. Fee, E.J., "Digital Computer Programs for Estimating Primary Production, Integrated over Depth and Time, in Water Bodies," Special Report No. 14, University of Wisconsin-Milwaukee, Center for Great Lakes Studies, 1971.

9. Ryther, J.H., and Yentsch, C.S., "The Estimation of Phytoplankton Production in the Ocean from Chlorophyll and Light Date," Limnology and Oceanography, Vol. 2, 1957.

10. Kiefer, D., and Strickland, J.D.H., "A Comparative Study of Photosynthesis in Seawater Samples Incubated Under Two Types of Light Attenuators," Limnology and Oceanography, Vol. 15, 408-412, 1970.

11. Hellebust, J.A. , and Terborgh, J., "Effects of Environmental Conditions on the Rate of Photosynthesis and Some Photosynthetic Enzymes in Dunaliella Tertiolecta Butcher," Limnology and Oceanography, Vol. 12, No. 4, 559-567, 1967.

12. Talling, J.F., "Comparative Laboratory and Field Studies of Photosynthesis by a Marine Planktonic Diatom," Readings in Aquatic Ecology, edited by Ford, R.F., and Hazen, W.E., W.B. Saunders Company, Philadelphia, 3-18, 1972.

13. Riley, G.A., "Factors Controlling Phytoplankton Populations of Georges Bank," Readings in Aquatic Ecology, edited by Ford, R.F., and Hazen, W.E., W.B. Saunders Company, Philadelphia, 227-242, 1972.

14. McAllister, C.D., Parsons, T.R., Stephens, K., and Strickland, J.D.H., "Measurements of Primary Production in Coastal Sea Water Using a Large-Volume Plastic Sphere," Readings in Aquatic Ecology, edited by Ford, R.E., and Hazen, W.E., W.B. Saunders Company, Philadelphia, 243-264, 1972.

15. Wright, J.C., "Limnology of Canyon Ferry Reservoir II. Phytoplankton Standing Crop and Primary Production," Reading in Aquatic Ecology, edited by Ford, R.F., and Hazen, W.E., W.B. Saunders Company, Philadelphia, 265-275, 1972.

16. Wezernak, C.T., Lyzehga, D.R., and Polcyn, F.C., "Remote Sensing Studies in the New York Bight," Final Report, Environmental Research Institute of Michigan, Ann Arbor, Michigan, Report No. 109300-5-F, 1975.

17. Dake, M.K., and Harleman, R.F., "An Analytical and Experimental Investigation of Thermal Stratifications in Lakes and Ponds," Report No. 99, Massachusetts Institute of Technology, Hydrodynamic Laboratory, 1966.

18. Huber, W.C., and Harleman, R.F., "Laboratory and Analytical Studies of the Thermal Stratifications of Reservoirs," Report No. 112, Massachusetts Institute of Technology, Hydrodynamic Laboratory, 1968.

19. Dake, M.K., and Harleman, R.F., "Thermal Stratification in Lakes, Analytical and Laboratory Studies," Water Resources Research, Vol. 5, No. 2, 484-495, 1969.

20. Ou, Jenn-Wu, Tinney, E.R., and Yang, Wen-Jei, "Thermal Stratification in Deep Reservoirs Due to Solar Radiation," Presented at the ASME Joint Applied Mechanics and Fluid Engineering Conference, 1973.

21. Orlob, G.T., and Selna, L.G., "Temperature Variation in Deep Reservoirs," Journal of Hydraulics Division, Proceedings of the American Society of Civil Engineers, Vol. 96, No. HY2, 391-410, 1970.

22. Shonting, D.H., "Some Observations of Short-Term Heat Transfer Through the Surface Layers of the Ocean," Limnology and Oceanography, Vol. 9, 576-588, 1965.

23. Foster, T.D., "A Convective Model for the Diurnal Cycle in the Upper Ocean," Journal of Geophysical Research, Vol. 76, No. 3, 666-675, 1971.

24. Snider, M.D., "An Experimental and Analytical Study of Thermal Structure in Heated and Cooled Stagnant Waters," Master Thesis, Purdue University, 1973.

25. Hill, R.G., and Viskanta, R., "An Unsteady Three Dimensional Model for Temperature Distribution in Rivers with Thermal Discharge," Paper 62C, Presented at the American Institute of Chemical Engineers National Meeting in Houston, Texas, March 1975.

26. Lepper, S.P., "Diurnal Solar Heating and Cooling of a Water Reservoir," M.S. Thesis, University of Missouri-Rolla, Rolla, Missouri, 1974.

27. Sundaram, T.R., and Rehm, R.G., "Formation and Maintenance of Thermoclines in Temperate Lakes," AIAA Journal, Vol. 9, No. 7, 1322-1329, 1970.

28. Dingman, S.L., "Equilibrium Temperatures of Water Surfaces as Related to Air Temperature and Solar Radiation," Water Resources Research, Vol. 8, No. 1, 42-49, 1972.

29. Beard, J.T., and Hollen, D.K., "The Influence of Solar Radiation Reflectance on Water Evaporation," J. Geophys. Res., Vol. 75, 5155-5162, 1970.

30. Pierson, R.W., and Jackman, A.P., "An Investigation of Several Evaporative Equations," Journal of Applied Meteorology, Vol. 14, No. 4, 477-487, 1975.

31. Lambeux, W.W., "Modern Evaporation Formulae Adapted to Computer Use," Monthly Weather Review, 26-28, Jan. 1962.

32. Schooley, A.H., "Evaporation in the Laboratory and at Sea," Journal of Marine Research, Vol. 27, No. 3, 335-338, 1969.

33. Paily, P.P., Macagno, E.O., and Kennedy, J.F., "Winter Regime Surface Heat Loss from Heated Streams," Institute of Hydraulic Research, IIHR Report No. 155, Iowa, March 1974.

34. Idso, S.B., and Cole, G.A., "Studies on a Kentucky Knobs Lake," Some Aspects of the Vertical Transport of Heat in the Hypolimnion," Journal of Ecology, No. 61, 413-420, 1973.

35. Sweers, H.E., "Vertical Diffusivity Coefficient in a Thermocline," Limnology and Oceanography, Vol. 15, 273-280, 1970.

36. Powell, T. and Jassby, A., "The Estimation of Vertical Eddy Diffusivity Below the Thermocline in Lakes," Water Resources Research, Vol. 10, No. 2, 191-198, 1974.

37. Liggett, J.A., "Unsteady Circulation in Shallow, Homogeneous Lakes," Journal of the Hydraulics Division, ASCE, Vol. 95, No. HY4, 6454-6461, 1969.

38. Janowitz, G.S., "The Effect of Finite Vertical Ekman Number on the Coastal Boundary Layer of Lakes," Tellus XXII, 5, 414-420, 1972.

39. Janowitz, G.S., "The Coastal Boundary Layers of a Lake when the Horizontal and Vertical Ekman Numbers are of Different Orders of Magnitude," Tellus XXII, 6, 585-596, 1970.

40. Stefan, H. and Ford, D.E., "Temperature Dynamics in Dimictic Lakes," Journal of the Hydraulics Division, ASCE, Vol. 101, No. HY1, 97-114, 1975.

41. Wu, J., "Wind Stress and Surface Roughness at Air-Sea Interface," Journal of Geophysical Research, Vol. 74, No. 2, 444-455, 1969.

42. Sullivan, S.A., "Experimental Study of the Absorption in Distilled Water, Artificial Sea-Water, and Heavy Water in the Visible Range of the Spectrum," Journal of the Optical Society of America, Vol. 53, No. 8, 962-968, 1963.

43. Tyler, J.E., and Smith, R.C., "Spectroradiametric Characteristics of Natural Light Under Water," Journal of the Optical Society of America, Vol. 57, No. 5, 205-211, 1967.

44. Smith, R.C., and Tyler, J.E., "Optical Properties of Clear Natural Water," Journal of the Optical Society of America, Vol. 57, No. 5, 177-203, 1967.

45. Hulburt, E.O., "Optics of Distilled and Natural Water," Journal of the Optical Society of America, Vol. 35, No. 11, 1945.

46. Fairchild, H.N., "The Transfer of Radiation in Natural Waters," Ph.D. Thesis, North Carolina State University at Raliegh, 1973.

47. Thekaekara, M.P., "Proposed Standard Values of the Solar Constant and the Solar Spectrum," Journal of Environmental Sciences, Vol. 13, 6-8, 1970.

48. Thekaekara, M.P., "The Solar Constant and Spectral Distribution of Solar Radiant Flux," Journal of Solar Energy, Vol. 9, 7-20, 1965.

49. Threlkeld, J.L., and Jordan, R.C., "Direct Solar Radiation Available on Clear Days," Journal of Heating, Piping and Air Conditioning, December 1957.

50. Gast, P.R., "Solar Radiation," Handbook of Geophysics, McMillan Co., New York, 1960.

51. Born, M. and Wolf, E., Optics, Addison-Wesley, New York, 1950.

52. Armaly, B.F. and Lam, T.T., "Influence of Refractive Index on Reflectance from a Semi-Infinite Absorbing Scattering Medium with Collimated Incident Radiation," International Journal of Heat and Mass Transfer, Vol. 19, 893-900, 1975.

53. Armaly, B.F. and Lam, T.T., "A Note on the Exponential Kernel Approximation," Journal of Quantitative Spectroscopy and Radiative Transfer, Vol. 13, 651-656, 1973.

54. Armaly, B.F. and Lam, T.T., "A Note on the Interface Functions," Journal of Quantitative Spectroscopy and Radiative Transfer, Vol. 13, 813-820, 1973.

55. Irving, W.M. and Pollack, J.B., "Infrared Optical Properties of Water and Ice Spheres," Icarus, Vol. 8, 518-528, 1958.

56. Armaly, B.F., Crosbie, A.L., Look, D.C. and Nelson, H.F., "Thermal Radiative Properties of a Smooth Air-Water Interface," International Journal of Heat and Mass Transfer, Vol. 16, 1477-1487, 1973.

57. Hulburt, E.O., "Optics of Distilled and Natural Water," Journal of the Optical Society of America, Vol. 35, 1945.

58. Idso, S.B., and Jackson, R.D., "Thermal Radiation from the Atmosphere," Journal of Geophysical Research, Vol. 74, No. 23, 5397-5403, 1969.

59. Duffie, J.A., and Beckman, W.A., "Solar Energy Thermal Processes," John Wiley & Sons, 1974.

60. Kraus, E.B. and Turner, J.S., "A One Dimensional Model of the Seasonal Thermocline," Tellus XIX, 88-106, 1967.

61. F.A.A. Flight Service Station Vichy, MO Surface Westher Observations, April 1975.

VITA

David Allen Prouty was born on May 8, 1952, in Jefferson City, Missouri. He received a Bachelor of Science degree from the University of Missouri-Rolla in December of 1973. While enrolled as an undergraduate he became a member of Phi Eta Sigma, Pi Tau Sigma, and Tau Beta Pi.

He has been enrolled in the Graduate School of the University of Missouri-Rolla since January of 1975. While enrolled he was a Graduate Teaching Assistant and a Graduate Research Assistant.

He is currently enrolled in the Graduate School of the University of Missouri-Rolla as a Doctoral student.